The Future of Heterodyne Detection in Space

- Heterodyne detection
  - used for $\lambda = 1$ cm to 100 μm
  - limited by quantum noise, $Tn \sim h\nu/k$
  - no spectral resolution limit
- Direct Detection
  - limited by background noise
  - difficult to achieve full sensitivity and high resolution, simultaneously
- Direct detection preferable for low resolution –
- Heterodyne detection preferable for high resolution –

  } crossover ~ R = 1,000 – 10,000
- General point – High spatial resolution demands high spectral resolution (narrow lines)

Role in a Future Large-Aperture Mission

- Significantly expands scientific capability
  - Attracts broader community
- Effective follow-on to Herschel
  - 4-10x improvement in receiver sensitivity
  - 5x larger aperture (8m vs. 3.5m)
  - Wider bandwidth (3x ?)
- 10^3 faster for individual lines
- 10^4 faster for line surveys
- Better angular resolution !

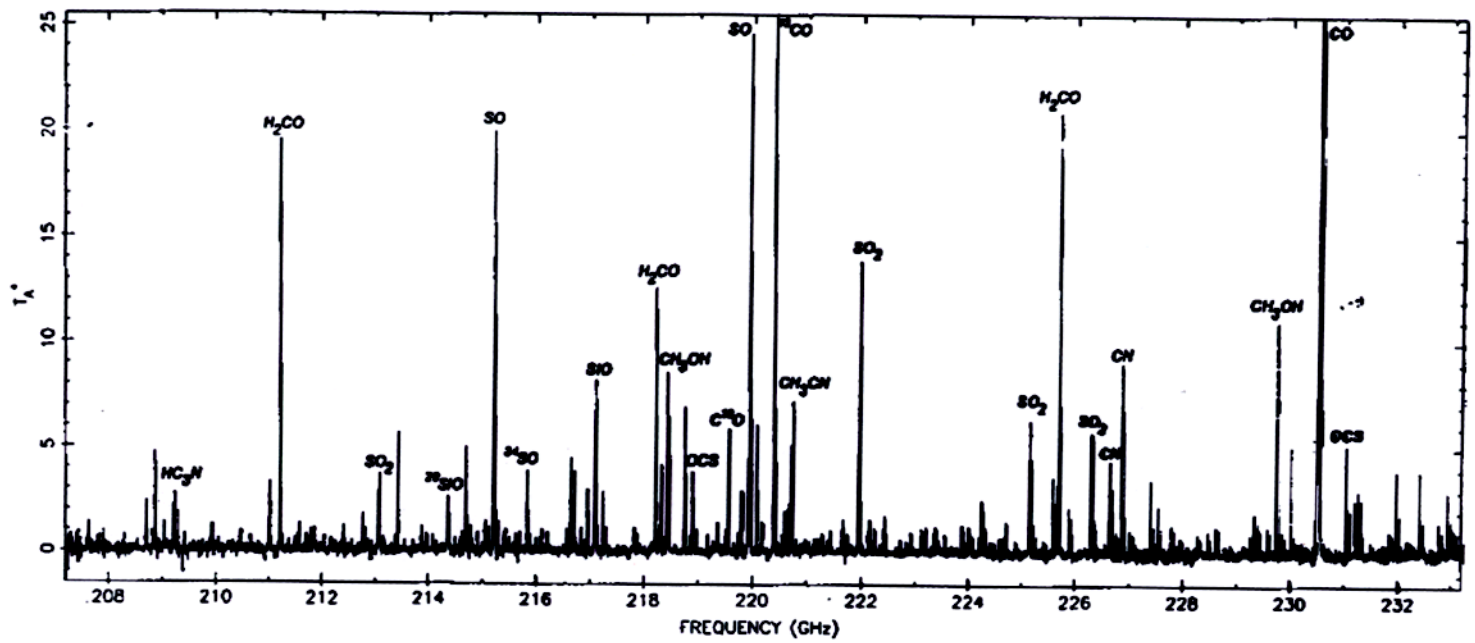

T_A^*
FREQUENCY (GHz)
H_2CO
SO
SO_2
^{28}SiO
^{34}SO
SiO
H_2CO
CH_3OH
OCS
$C^{18}O$
SO
^{13}CO
CH_3CN
SO_2
H_2CO
SO_2
SO_2
CN
CN
CH_3OH
CO
OCS
HC_3N

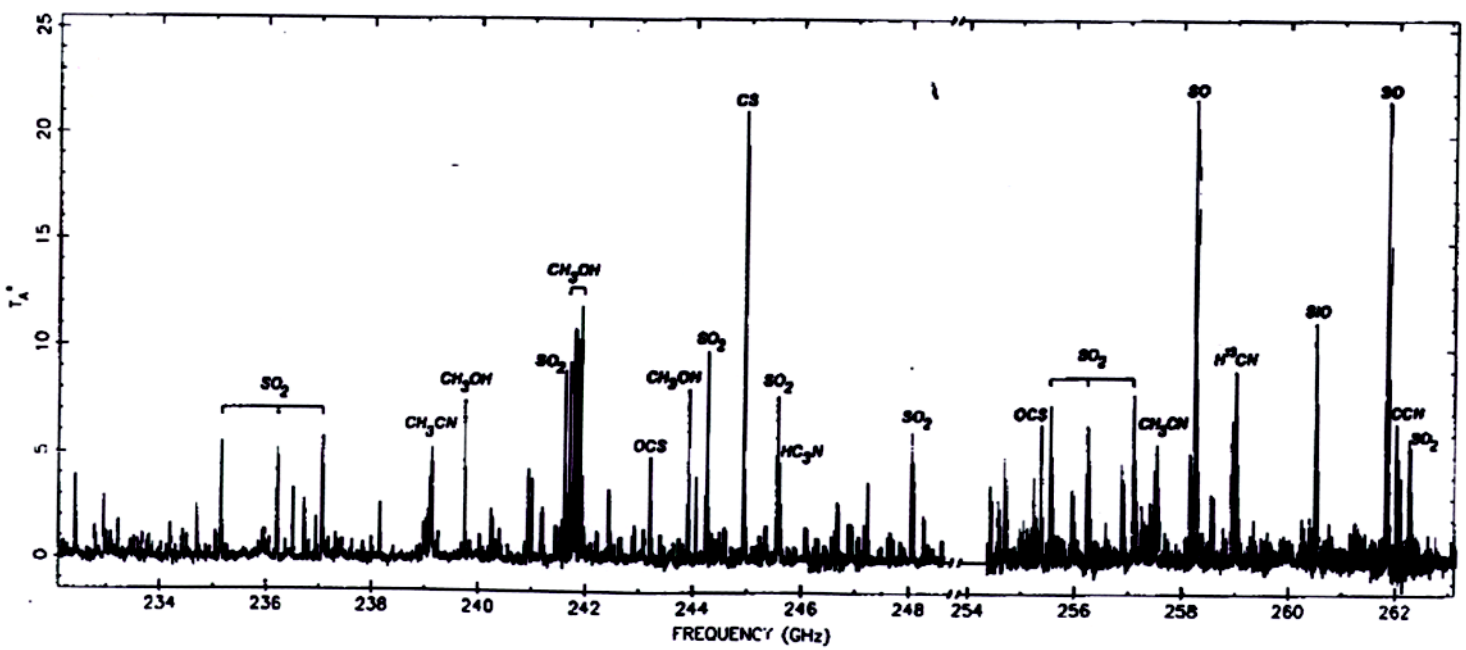

T_A^*
FREQUENCY (GHz)
SO_2
CH_3CN
CH_3OH
SO_2
CH_3OH
OCS
CH_3OH
SO_2
CS
SO_2
HC_3N
SO_2
OCS
SO_2
CH_3CN
SO
$H^{13}CN$
SiO
SO
CCH
SO_2

Figure I.2 Submillimeter spectrum of a cloud from Phillips and Keene (1992).

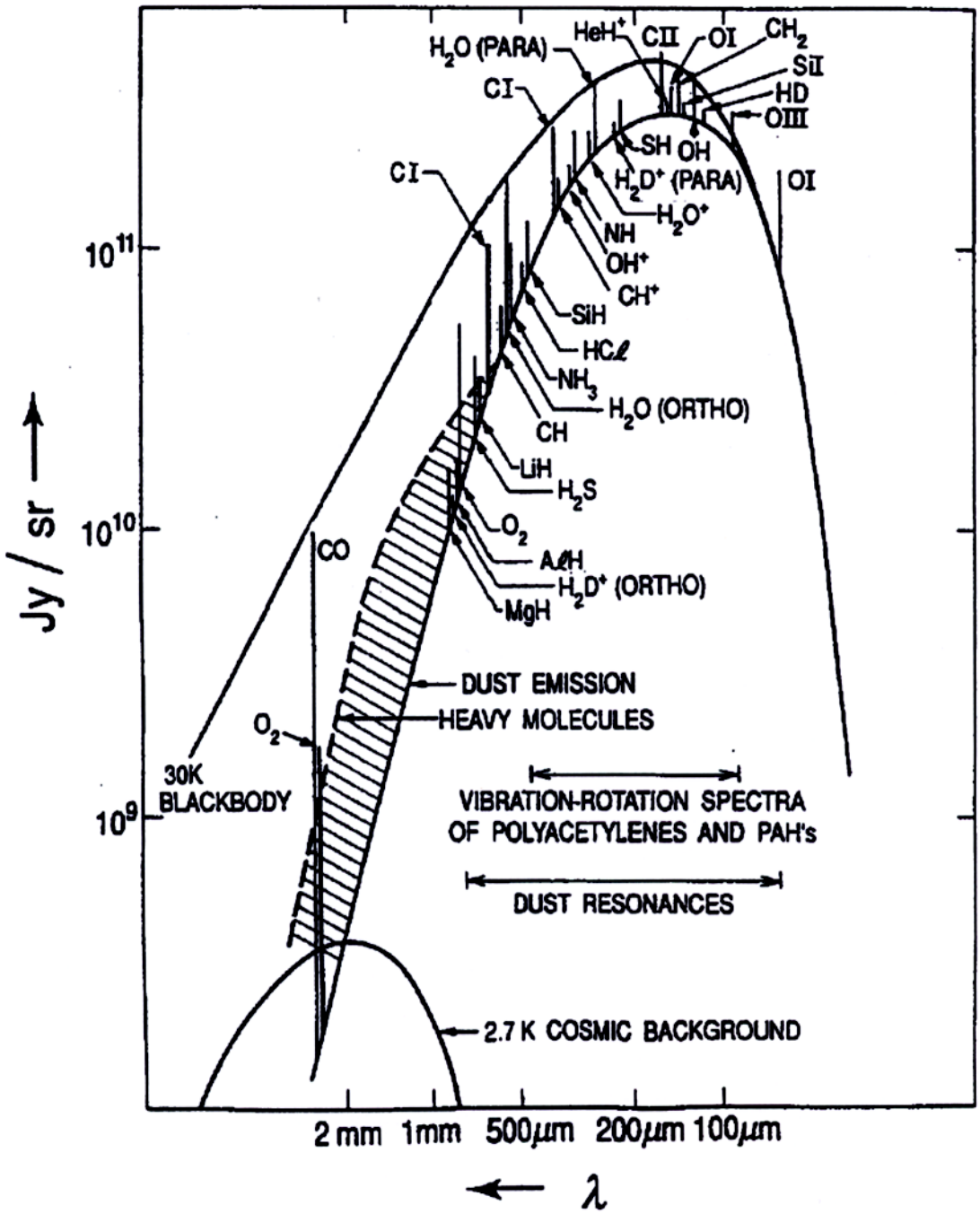

Submm/far-IR spectroscopy

- Interstellar chemistry
  - ground-state lines of interstellar hydrides
  - HD, H_2D^+
  - H_2O, $H_2{}^{18}O$, HDO, H_3O^+, OH
  - CH, CH_2, CH^+
  - HCl, HF
- Warm molecular gas: hot cores, shocks, and PDRs
  - high-J CO lines
  - fine-structure lines of N^+, C^+, C, O
- $R \sim 10^6$
  - Solar system
  - Evolved stars
  - Star formation, disks
- $R \sim 10^4 - 10^5$
  - Nearby galaxies
- $R \sim 10^3 - 10^4$
  - Redshifts for submm galaxies
  - Diagnostics for high-z galaxies

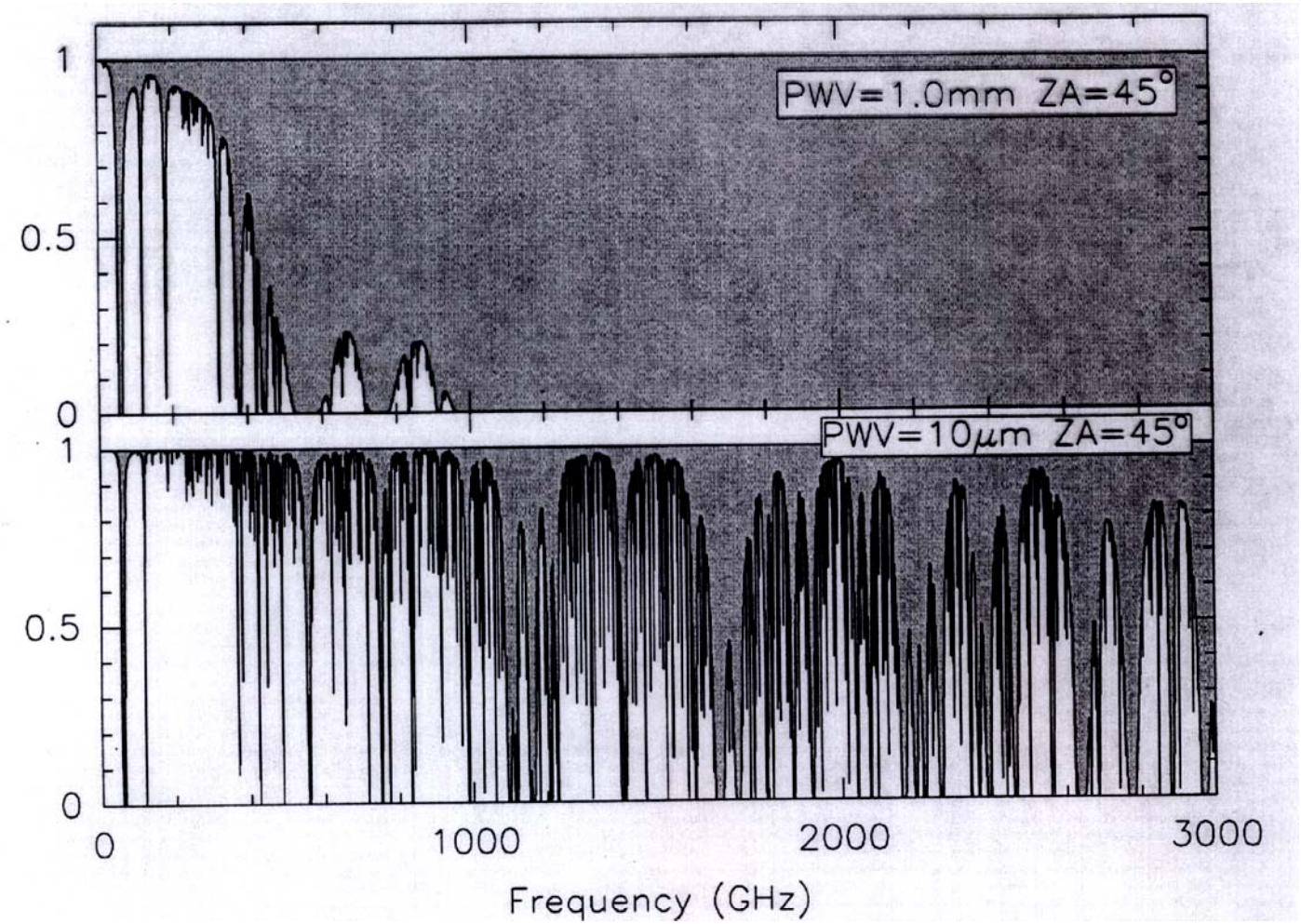
PWV=1.0mm ZA=45°
PWV=10μm ZA=45°
1
0.5
0
1
0.5
0
0
1000
2000
3000
Frequency (GHz)

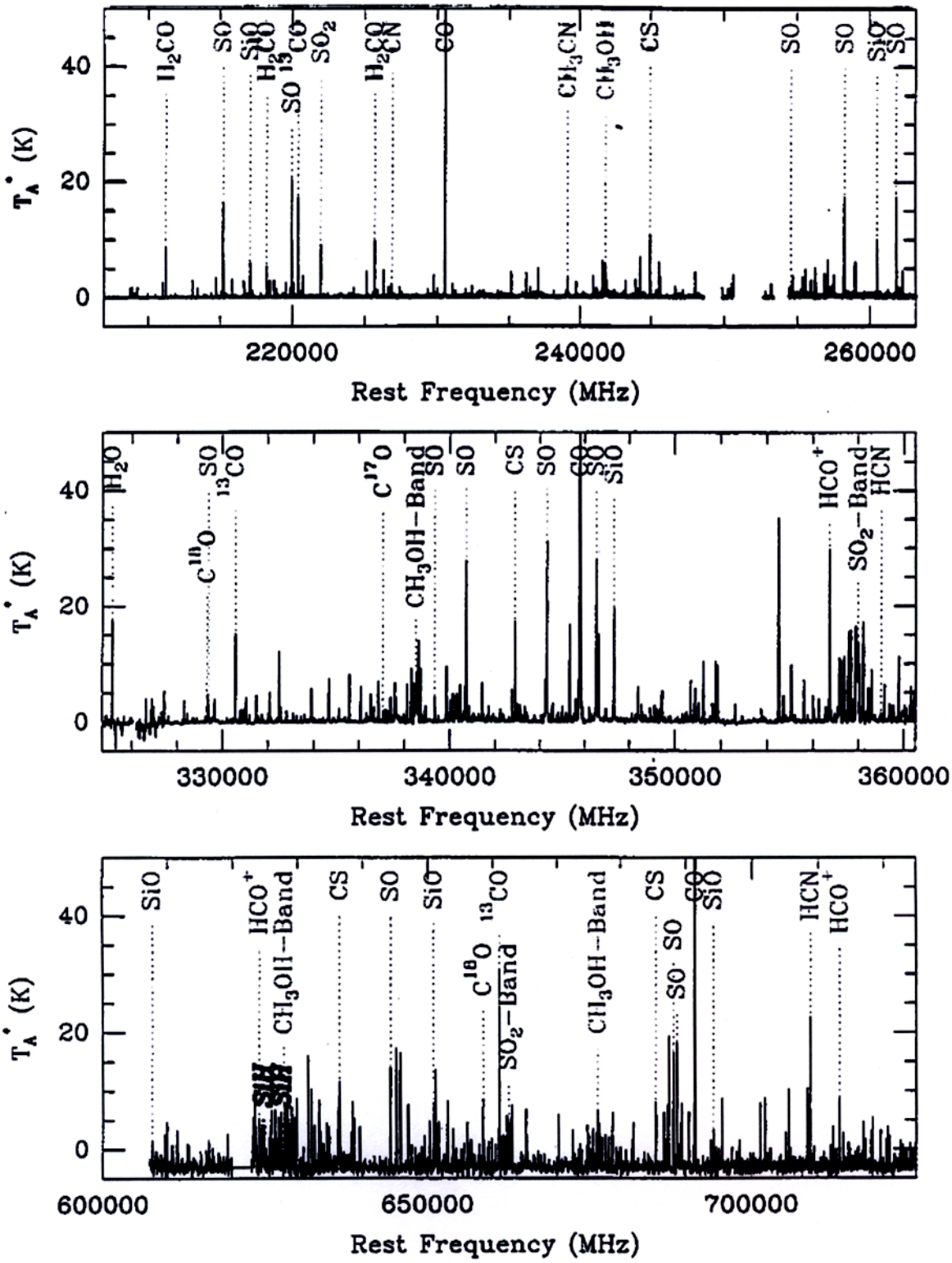
T_A^* (K)
Rest Frequency (MHz)
H_2CO
SO
SiO
H_2CO
^{13}CO
SO_2
H_2CO
CN
CO
CH_3CN
CH_3OH
CS
SO
SiO
SO
H_2O
$C^{18}O$
^{13}CO
$C^{17}O$
CH_3OH-Band
CS
HCO^+
SO_2-Band
HCN
^{13}CO
$C^{18}O$
SO_2-Band
CH_3OH-Band
HCO^+

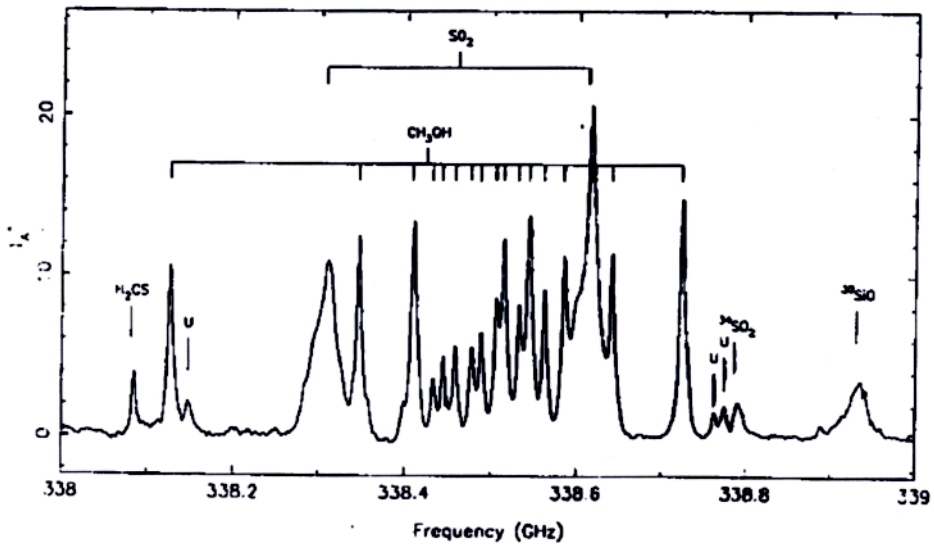

A 1 GHz section of the CSO line survey of Orion A showing the detail available after reduction to single sideband form. The original DSB observations had a back end width of 500 MHz.

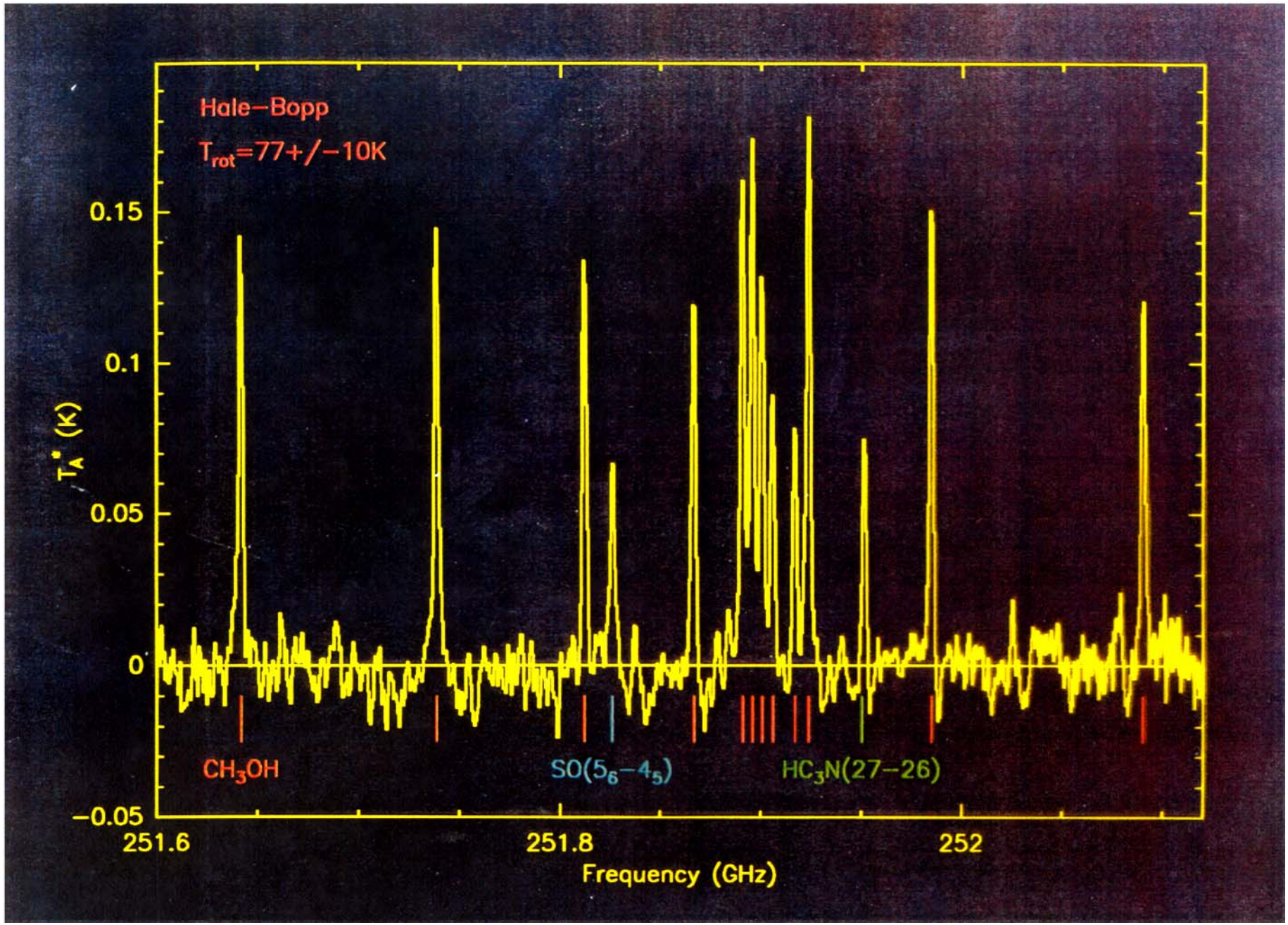
Hale–Bopp
T_{rot}=77+/−10K
0.15
0.1
0.05
0
−0.05
T_A^* (K)
CH_3OH
$SO(5_6-4_5)$
$HC_3N(27-26)$
251.6
251.8
252
Frequency (GHz)

TABLE 5.1

SIGNIFICANT FLUX CONTRIBUTIONS BY SPECIES FOR ORION-KL

Species [a]	N_{lines}	$\int T_{MB}\, d\nu$ (K MHz)	Relative Contribution (% of Total Line Flux)
$SO_2^{\dagger}$	71	10396.8	28.2
SO_2	37	9623.1	26.1
$CO^{\dagger}$	4	5392.6	14.6
CO	1	4884.7	13.3
$SO^{\dagger}$	14	4813.7	13.1
SO	6	3920.5	10.6
$CH_3OH^{\dagger}$	106	4196.5	11.4
CH_3OH	75	4029.9	10.9
$HCN^{\dagger}$	4	2492.8	6.8
HCN	1	1578.9	4.3
$HCOOCH_3$	211	1446.5	3.9
$SiO^{\dagger}$	3	911.4	2.5
$CH_3CN^{\dagger}$	35	898.5	2.4
$HCO^{+\,\dagger}$	3	771.2	2.1
$CS^{\dagger}$	3	535.7	1.5
CH_3OCH_3	82	406.9	1.1
U-lines	184	1625.2	4.4

[a] Values for species marked with a † also include the contributions of all transitions detected from isotopomers and vibrationally excited states. In some cases entries are made separately for the main species and for all of the variants together, *e.g.*, $SO_2^{\dagger}$ and SO_2 are both shown.

{1004 lines, 34 species
{60 U lines

Thermal line width ~ .05 km/sec ~ 50 kHz

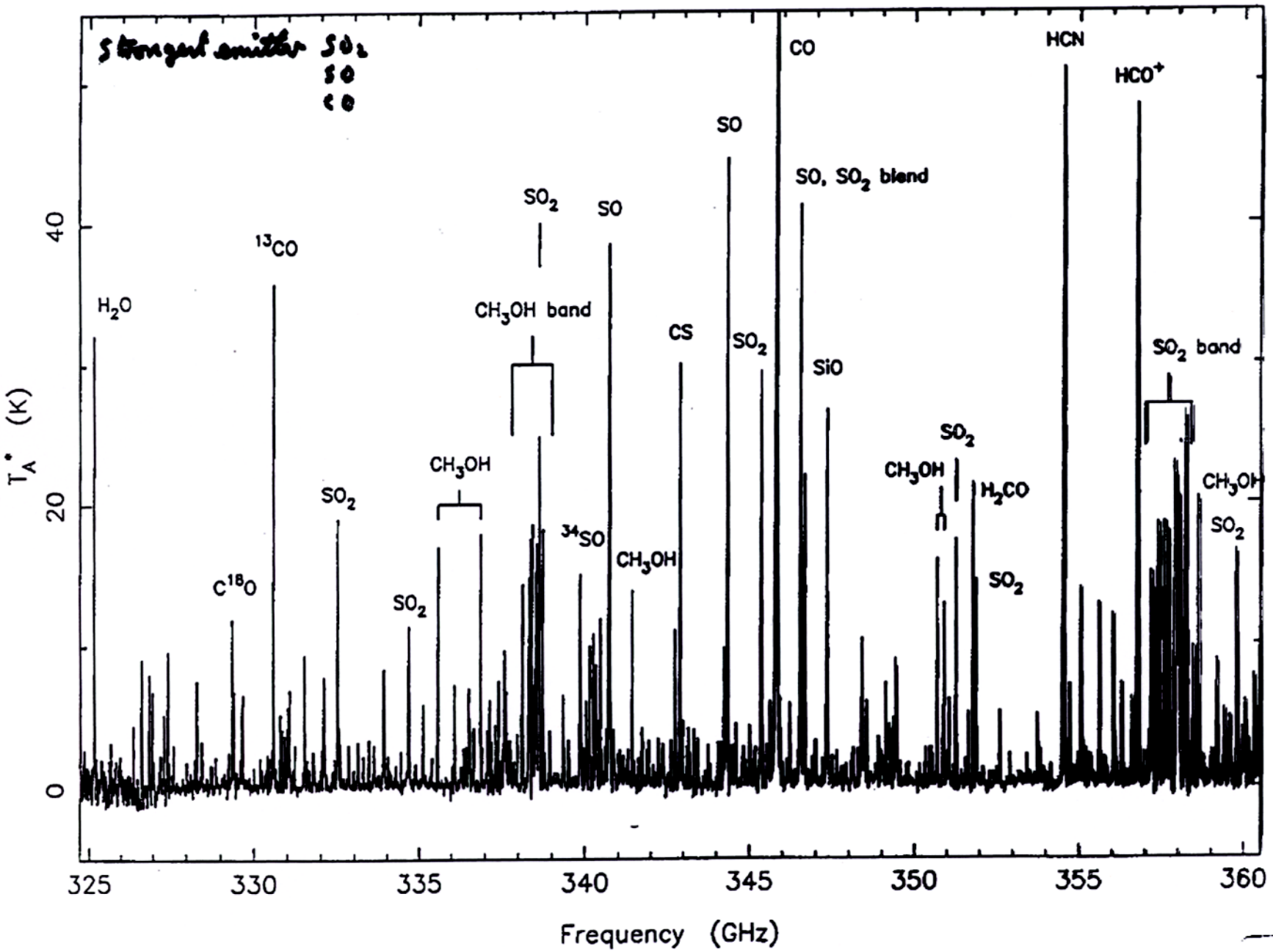

Fig. 5

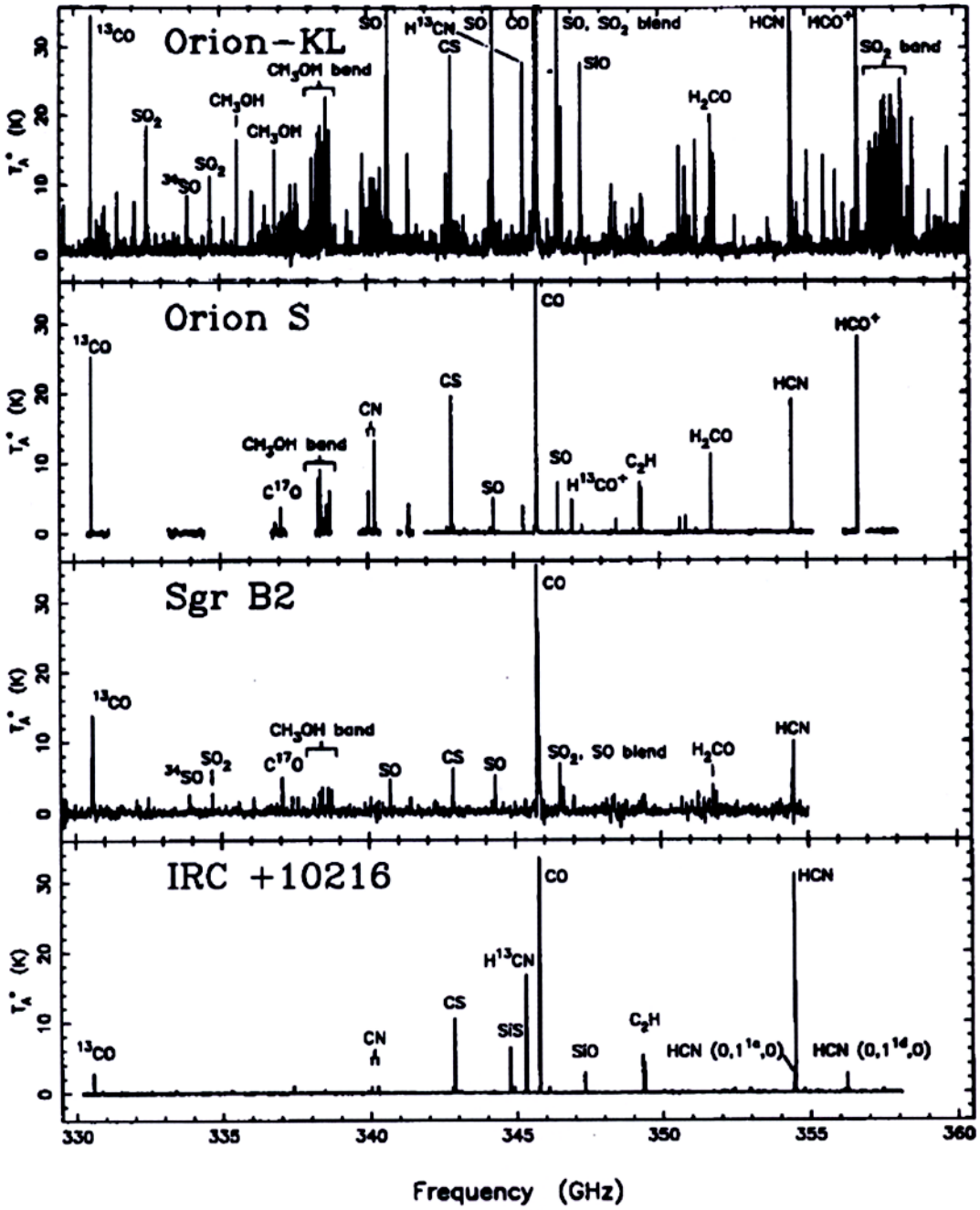

Figure IV1. Plot of the entire spectra between 325 and 360 GHz for SgrB2(M), Orion KL, and IRC+10216 (also shown for comparison is Orion 1.'5 S.) The strongest or most important lines are indicated. For Orion, we find 735 spectral features, of which 119 remain unidentified. Strong lines from linear rotors are the CS (7–6) line at 342.9 GHz, the HCN (4–3) line at 345.5 and the HCO^+ line at 356.7 GHz. Other noticeable spectral features are the strong CH_3OH 7–6 a–type transition band around 338.5 GHz, the corresponding band of torsionally excited CH_3OH ($v_t = 1$) at 337.7 GHz and the Q-branch band of SO_2 between 357 and 359 GHz. The comparative sparseness of the IRC+10216 survey is striking. Approximately 55 lines have been detected, with 3 remaining currently unidentified. For SgrB2(M), 128 resolved features were detected, with only a few lines being unidentified.

TABLE 5.13

SUMMARY OF LINE SURVEY FLUX RESULTS

Source	Frequency Range (GHz)	Coverage Achieved [a] (%)	Line Flux [b] (Jy)	Total Flux [c] (Jy)	Contribution of Line Flux (%)	Emissivity Index β [d]
Orion-KL	325–360	100	85	171 [e]	50	2.0 [f]
Orion-S	330–360	63	5.7	74 [e]	8	2.0 [f]
IRAS 16293–2422	330–360	50	0.9	17	5	1.0 [g]
IRC +10216	330–358	100	4.6	7.0 [h]	65	1.4 [i]
VY CMa	330–360	30	0.6	2.2	27	1.0 - 1.5 [j]
OH 231.8+4.2	330–360	30	0.5	2.2	23	1.0 - 1.5 [j]

[a] Fraction of the stated frequency range which was included in the observations.

[b] Values shown are the lower limits for the line flux (see the individual source discussions for details).

[c] Except as noted, the total flux values are taken from Sandell (1994).

[d] Estimated values for β after line flux corrections are made.

[e] Total flux values for Orion-KL and Orion-S are obtained from our observations.

[f] Based on data from Mezger *et al.* (1990).

[g] Based on data from Sandell (1994) and Mundy *et al.* (1992).

[h] Estimate based on our derived line flux and narrowband measurement of Sandell cited by Avery *et al.* (1992).

[i] Based on data from Sandell *et al.* (1994) and Sopka *et al.* (1985).

[j] Uncertain because of large spread in possible line flux correction; based on data from Sandell *et al.* (1994) Knapp *et al.* (1993).

^{12}CI & ^{13}CI

^{12}C and ^{13}C ($^3P_2 - {}^3P_1$) near the Orion Bar
Observed with the CSO 850 GHz receiver

Keene, et al

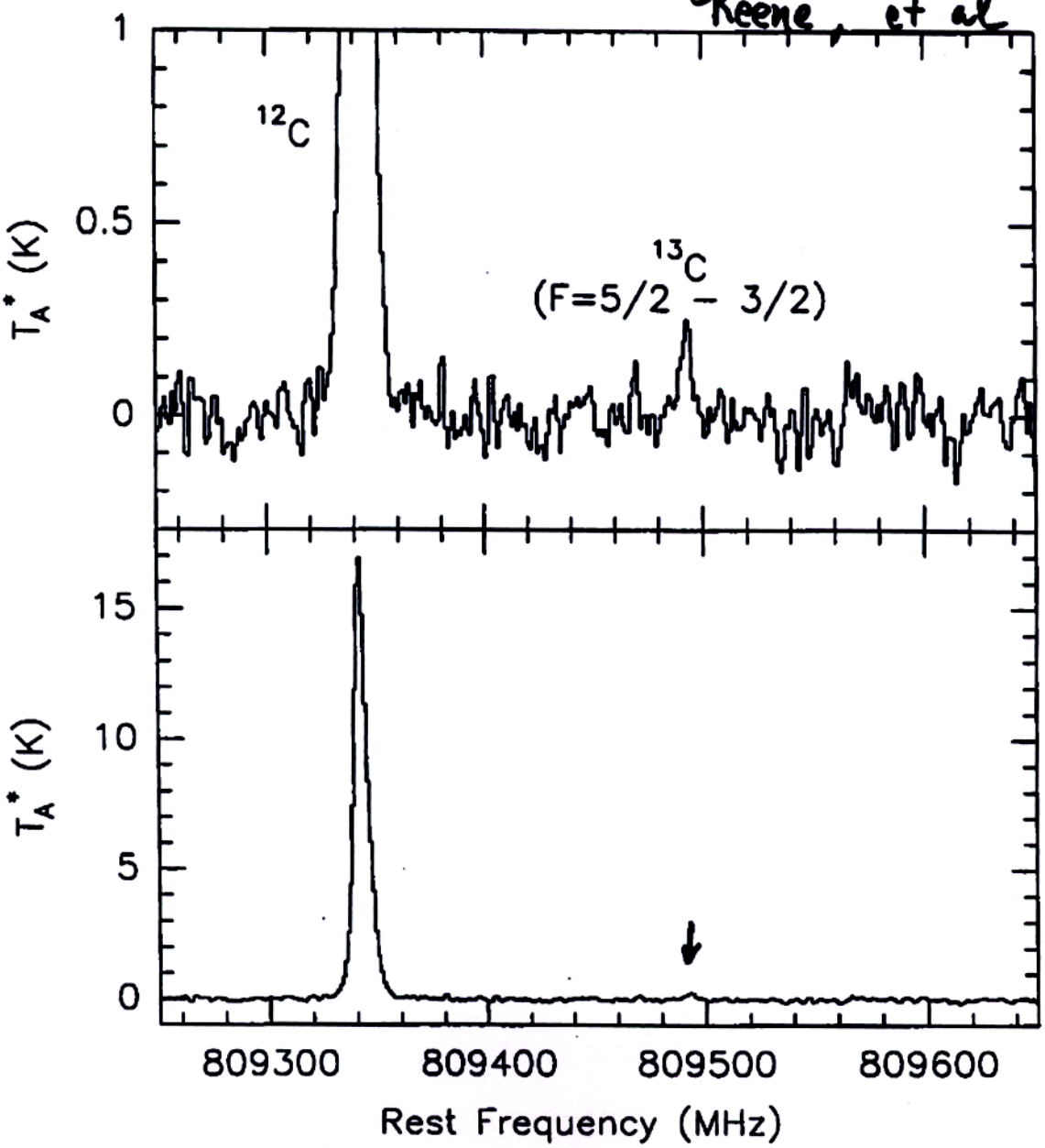

J. Keene et al. – 2 Feb 1997

CSO

HCl (1-0) - OMC-1

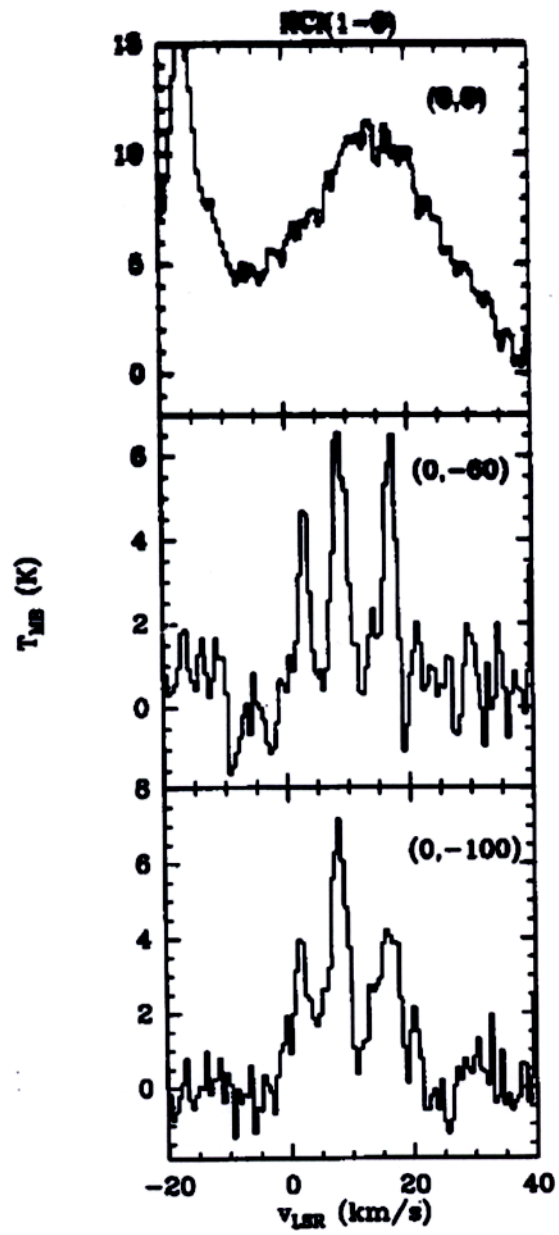

← Emission from Orion KL

← Emission from Ridge cloud.

Fig. 1.— Spectra of HCl(1–0) toward three representative positions. The offsets refer to $\alpha_{1950} = 5^h\,32^m\,46^s.7$, $\delta_{1950} = -5°\,24'24''$.

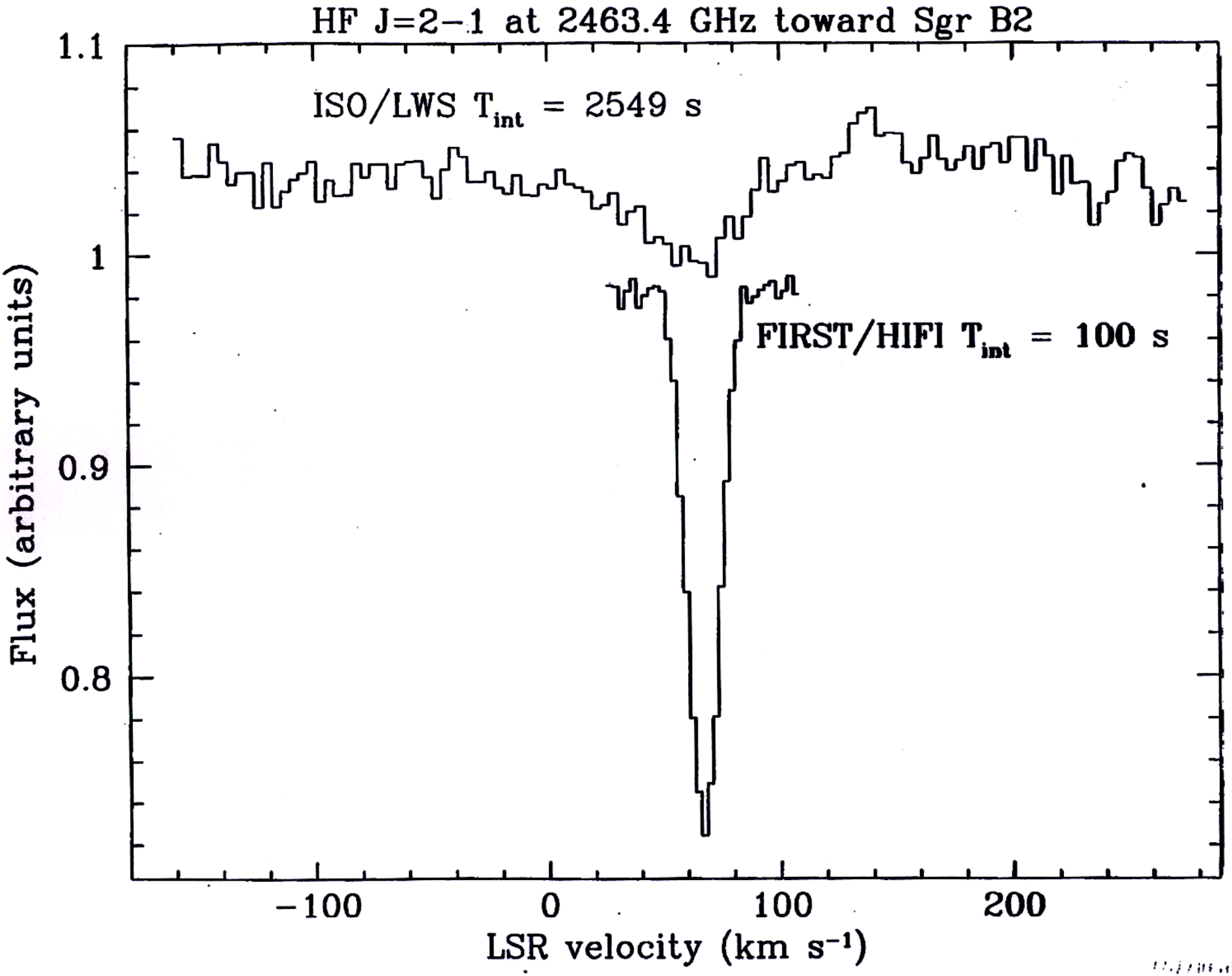
HF J=2−1 at 2463.4 GHz toward Sgr B2
ISO/LWS T_{int} = 2549 s
FIRST/HIFI T_{int} = 100 s
Flux (arbitrary units)
1.1
1
0.9
0.8
−100
0
100
200
LSR velocity (km s^{-1})

Even the CII 157 μm line !

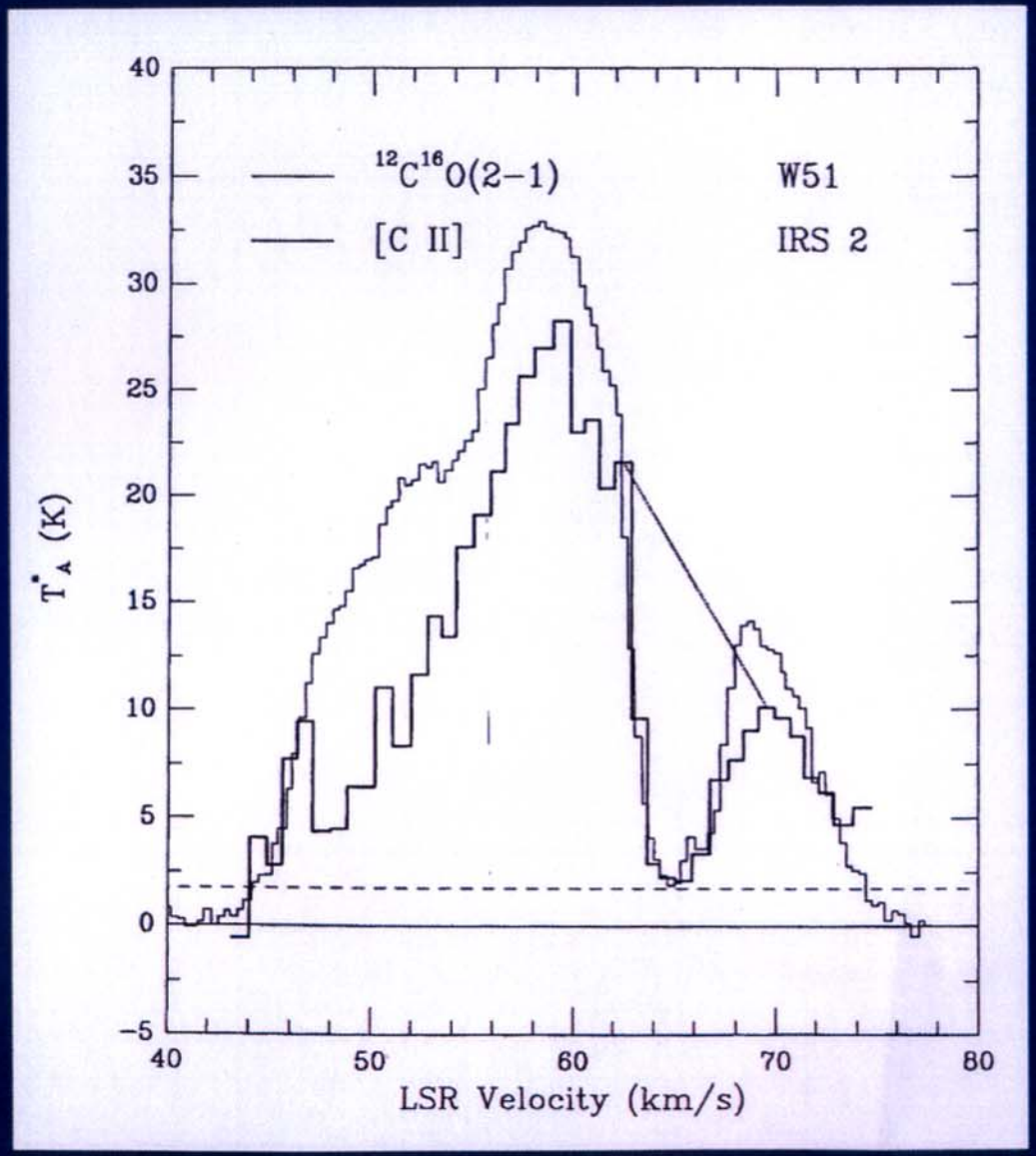

1987, KAO
Betz, Boreiko, Zmuidzinas

Massive star-formation region +
Low-density foreground PDR

Ground-state transition !

SWAS Observations in Orion

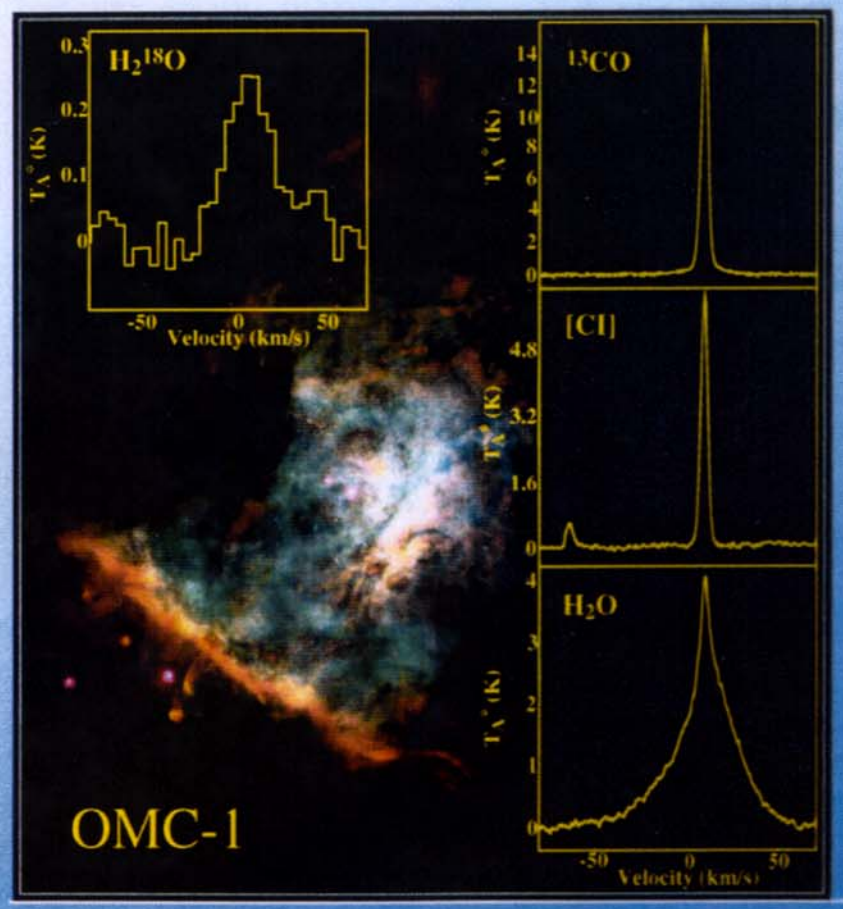

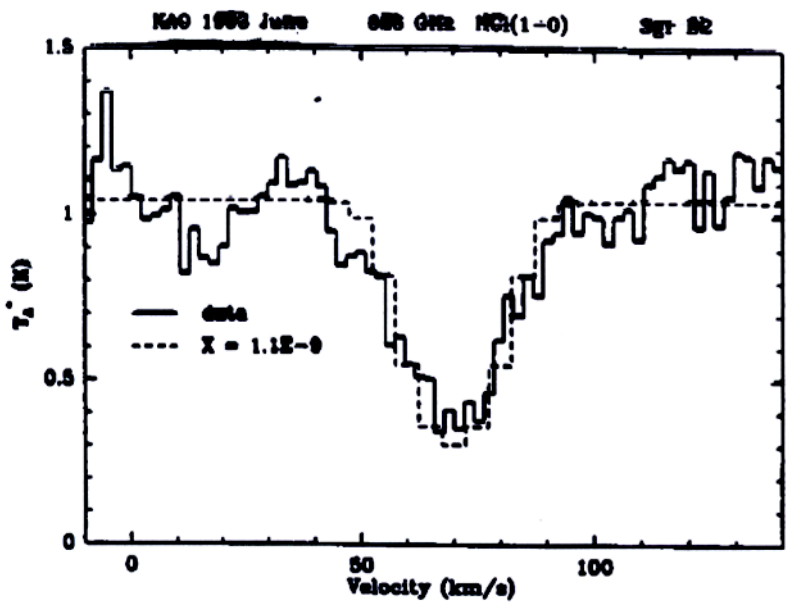

Fig. 2. Solid line: detection of the 626 GHz HCl line in absorption toward Sgr B2. Dashed line: spectrum predicted by our radiative transfer model for a fractional abundance of $HCl/H_2 = 1.1 \times 10^{-9}$.

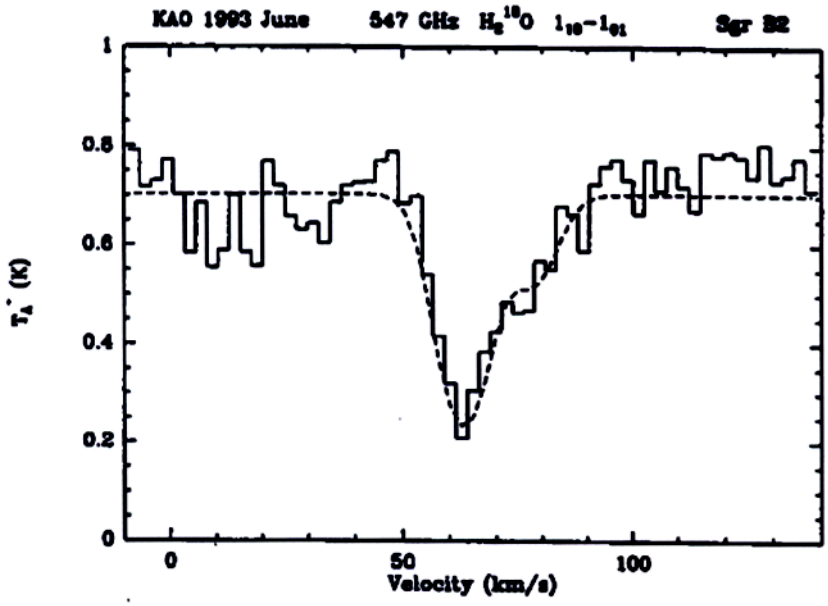

Fig. 3. The 547 GHz $H_2{}^{18}O$ transition detected in absorption in Sgr B2. The dashed line is the prediction of a simple model consisting of a background continuum source ($T_A^* \approx 0.7\ K$) and a foreground cloud with two velocity components. The *minimum* $H_2{}^{18}O$ column density capable of producing this absorption is about $1.1 \times 10^{14}\ cm^{-2}$.

Zmuidzinas et al.

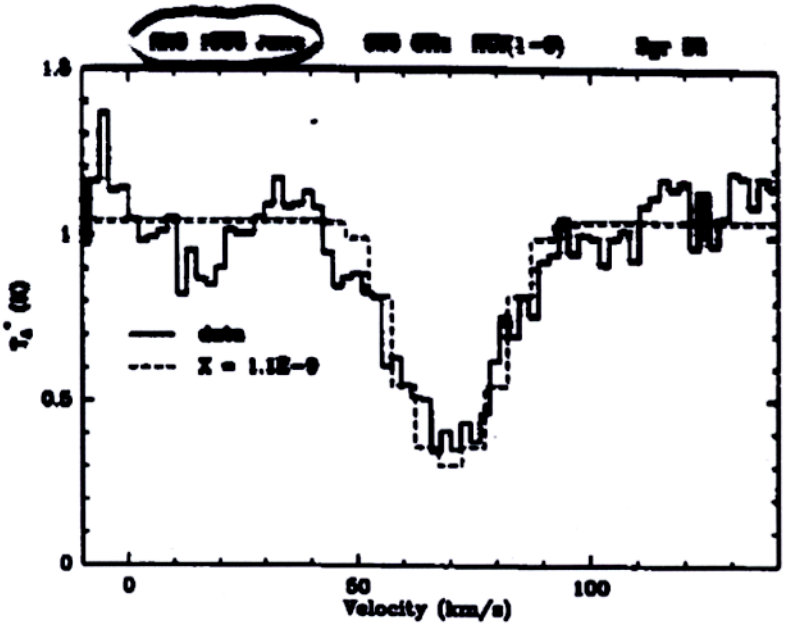

Fig. 2. Solid line: detection of the 626 GHz HCl line in absorption toward Sgr B2. Dashed line: spectrum predicted by our radiative transfer model for a fractional abundance of $HCl/H_2 = 1.1 \times 10^{-9}$.

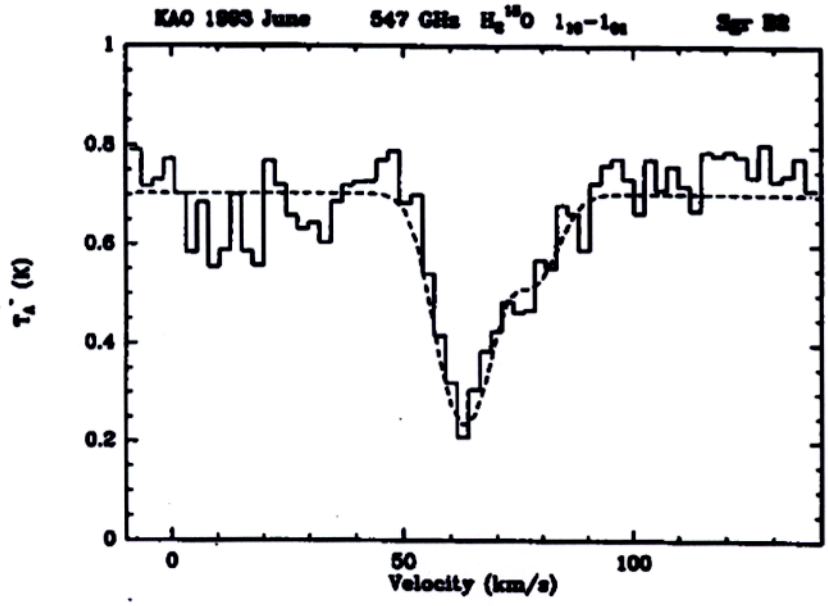

Fig. 3. The 547 GHz $H_2{}^{18}O$ transition detected in absorption in Sgr B2. The dashed line is the prediction of a simple model consisting of a background continuum source ($T_A^* \approx 0.7\ K$) and a foreground cloud with two velocity components. The *minimum* $H_2{}^{18}O$ column density capable of producing this absorption is about $1.1 \times 10^{14}\ cm^{-2}$.

Line profiles are often complex: H_2O at 557 GHz

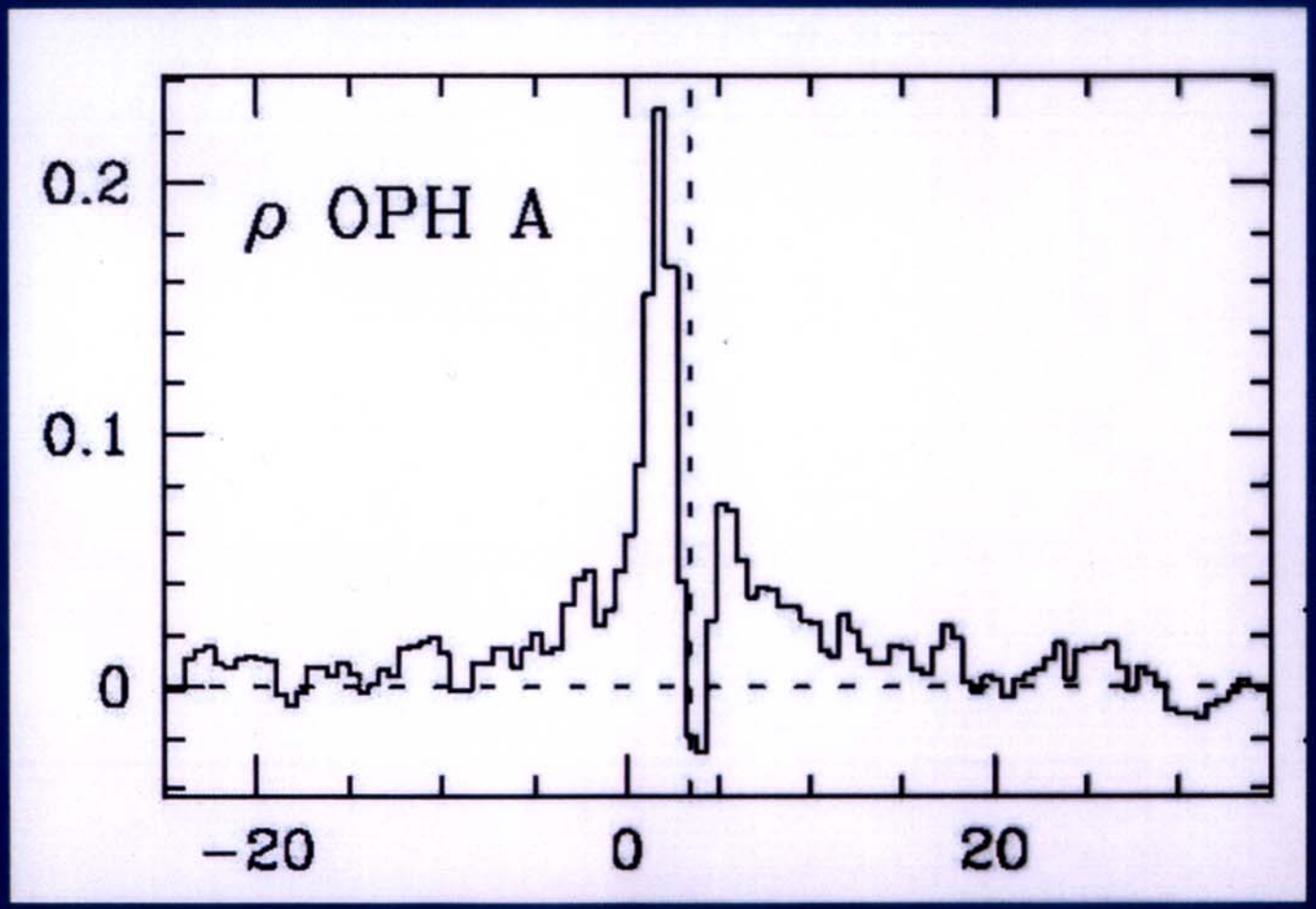

(Ashby et al., 2000; SWAS)

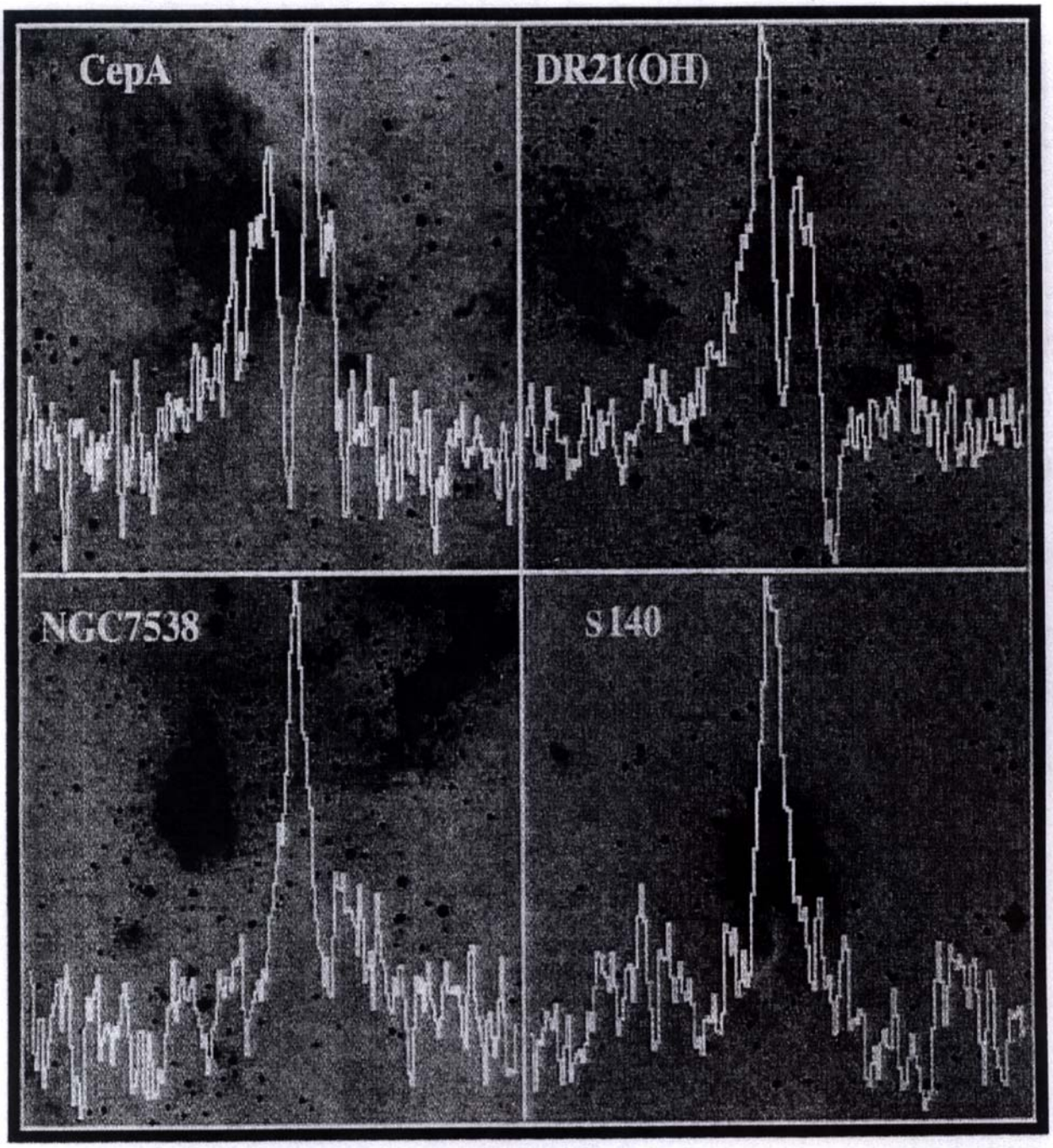

$H_2{}^{16}O$ Spectra Toward Four Galactic Star Forming Regions ($T_A{}^*$ ~ 0.2 - 0.3 K for these sources)

atmosphere. The primary constituents are O_2 (20.946% by volume), N_2 (78.084% by volume) and A(argon — 0.934% by volume). These constituents are well mixed up to a height of about 20 km, where the dissociation of molecular oxygen to atomic oxygen begins. Water vapor and ozone are added to the model atmosphere with distributions which vary with altitude. The maximum ozone density peaks near 25 km altitude with a value of about $5 \times 10^{12} cm^{-3}$. Water vapor exhibits an exponential decrease with altitude, with a scale height of 2 km, up to the level of the tropopause, above which the mixing ratio profile is usually taken to be constant.

Figure II.1 shows a calculation of the atmospheric transmission from an altitude of 12 km – typical of the KAO – for the entire frequency range of the Explorer. The calculation assumes a precipitable atmospheric water content of 10 μm. The number and strength of the absorption features is seen to increase with frequency. The extremely wide lines are due to water, the deep narrower lines are due to oxygen and the smaller sharp features are due in the main to ozone. From the altitude of 12 km it is not possible to make studies of the critical interstellar molecules H_2O and O_2 nor can we carry out spectroscopic surveys, galaxy line searches or sensitive continuum studies.

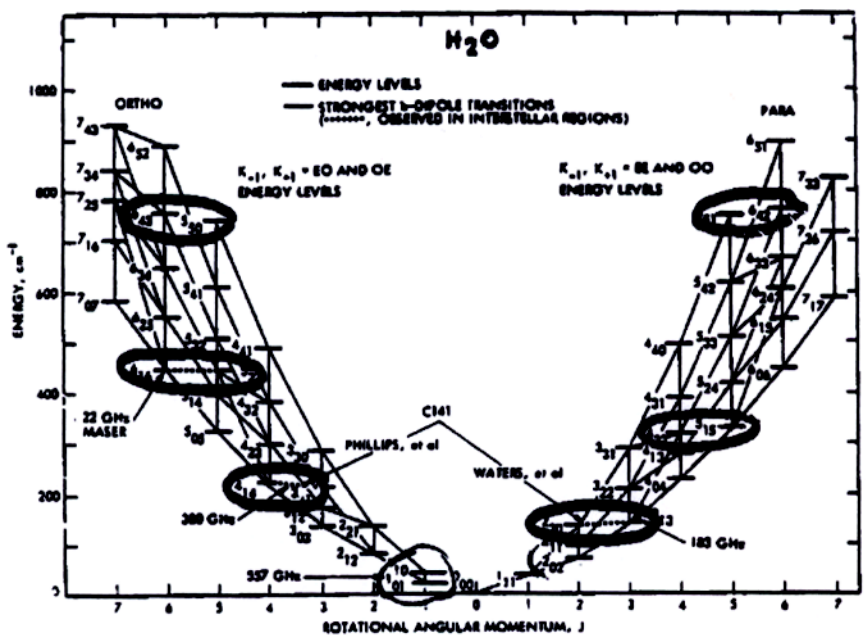

H_2O and $H_2{}^{18}O$ detections.

Figure II.2. — The ground rotational energy level diagram for H_2O.

B. H_2O and O_2 SPECTRA

Figures II-2 and II-3 indicate the submillimeter wavelength spectral features of the atmospherically blocked molecules, water vapor and oxygen. Together these molecules are predicted to contain the bulk

SWAS Observations in Orion

(H_2O)

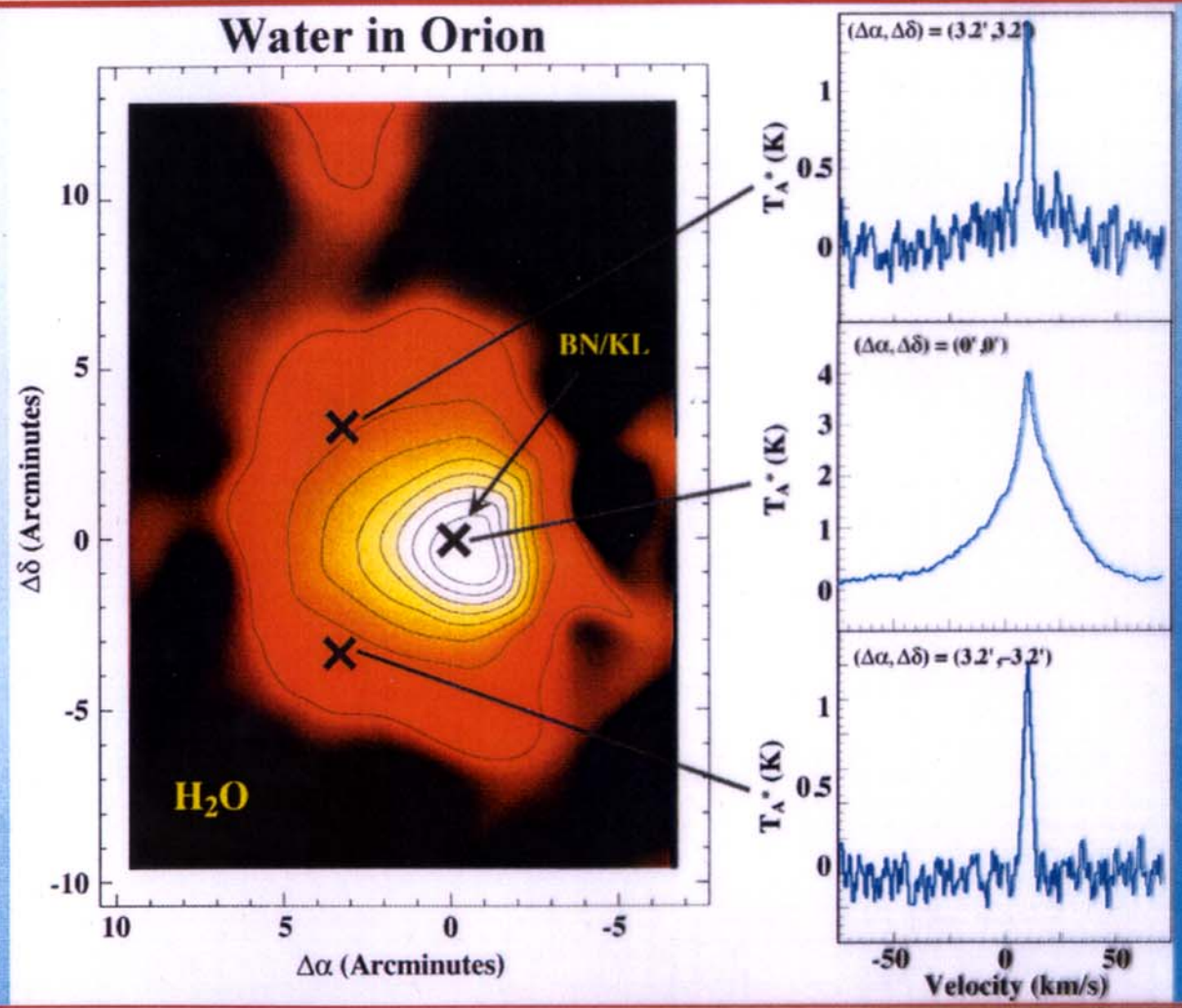

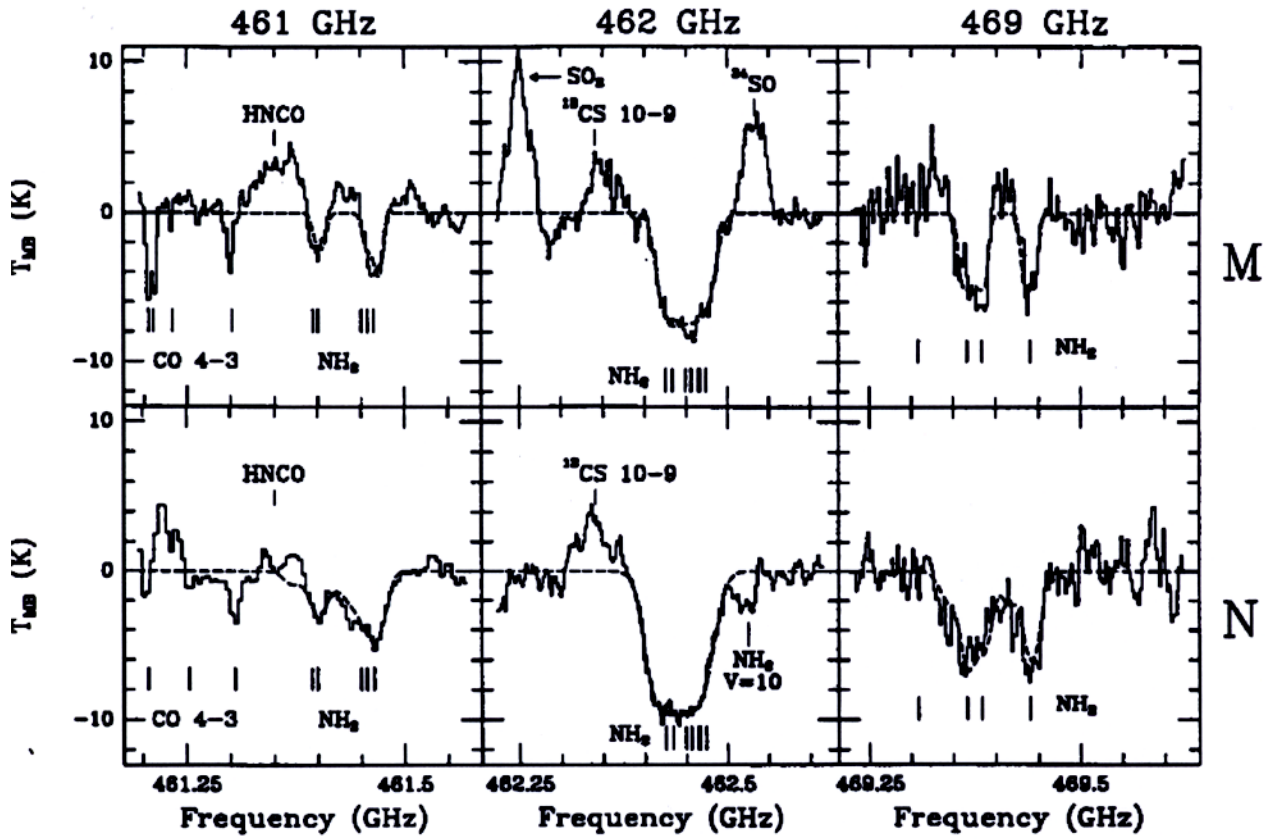

Figure 1. Spectra of NH_2 at 461, 462 and 469 GHz towards SgrB2(M) (top; $\alpha_{1950} = 17^h44^m10^s.6$, $\delta_{1950} = -28°22'05''$) and SgrB2(N) (bottom; $\alpha_{1950} = 17^h44^m10^s.6$, $\delta_{1950} = -28°21'20''$). The dashed lines are the hyperfine fits to the NH_2 lines. In the 461 GHz spectra, some CO 4–3 absorption features in spiral arm clouds are seen as well. NH_2 absorption at V_{LSR}=10 km s^{-1} is indicated in the 462 GHz spectrum towards SgrB2(N).

al. (1990) shows that the features seen in NH_2 basically trace the dust continuum, suggesting that there is no major variation of the NH_2 abundance over the map range. NH_2 thus seems to be a fairly widespread molecule which happens to be only easily observable in absorption towards strong continuum sources, for reasons of excitation.

$S/N \sim \frac{T_A}{T_N} \sqrt{\Delta\nu \Delta t}$ ~ 2,500 pixels in ~ 2 hrs.

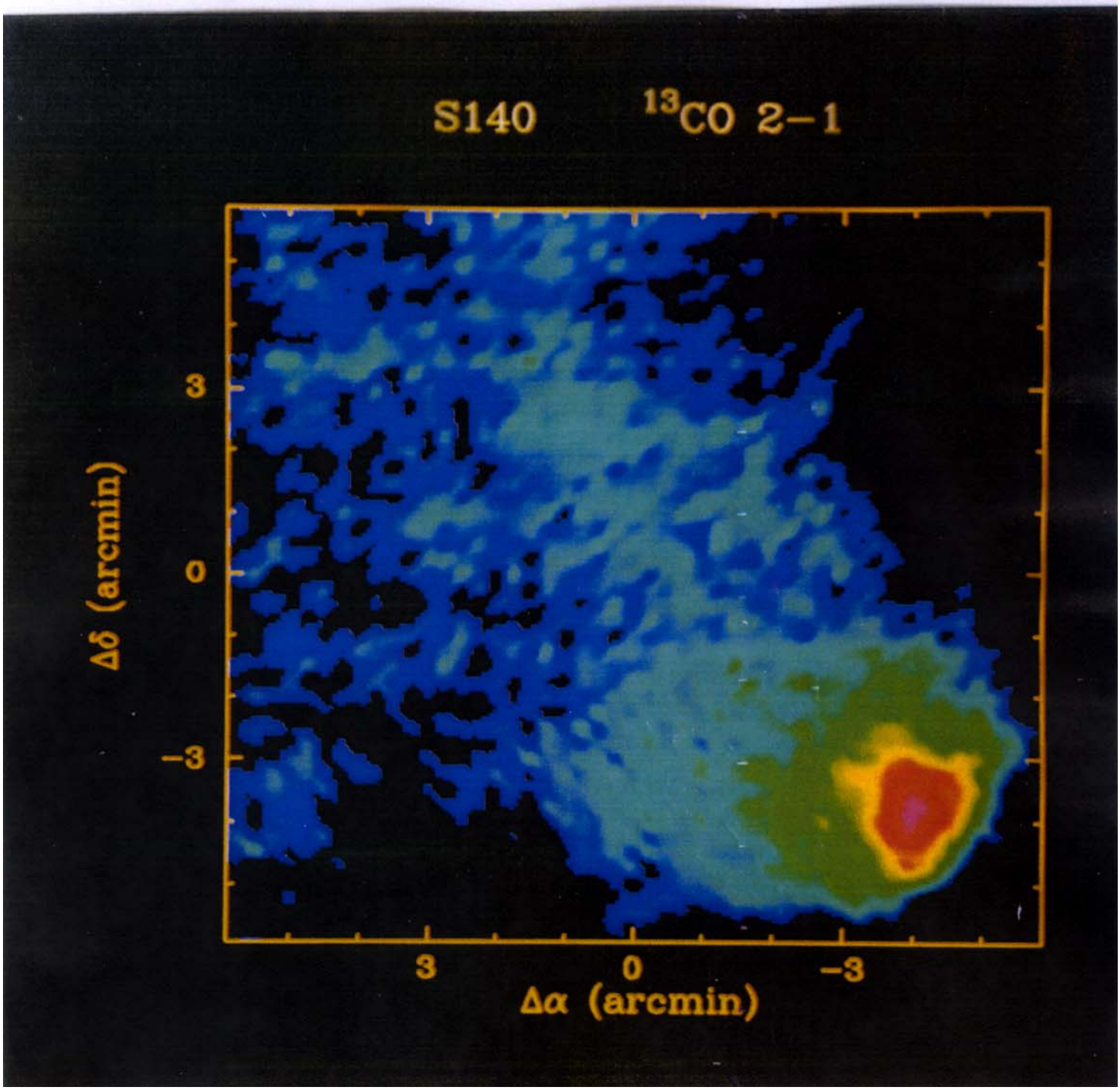

$t = 1.2\ \tau_{ac}$

(16)

non-compressible, small scale mode dominate

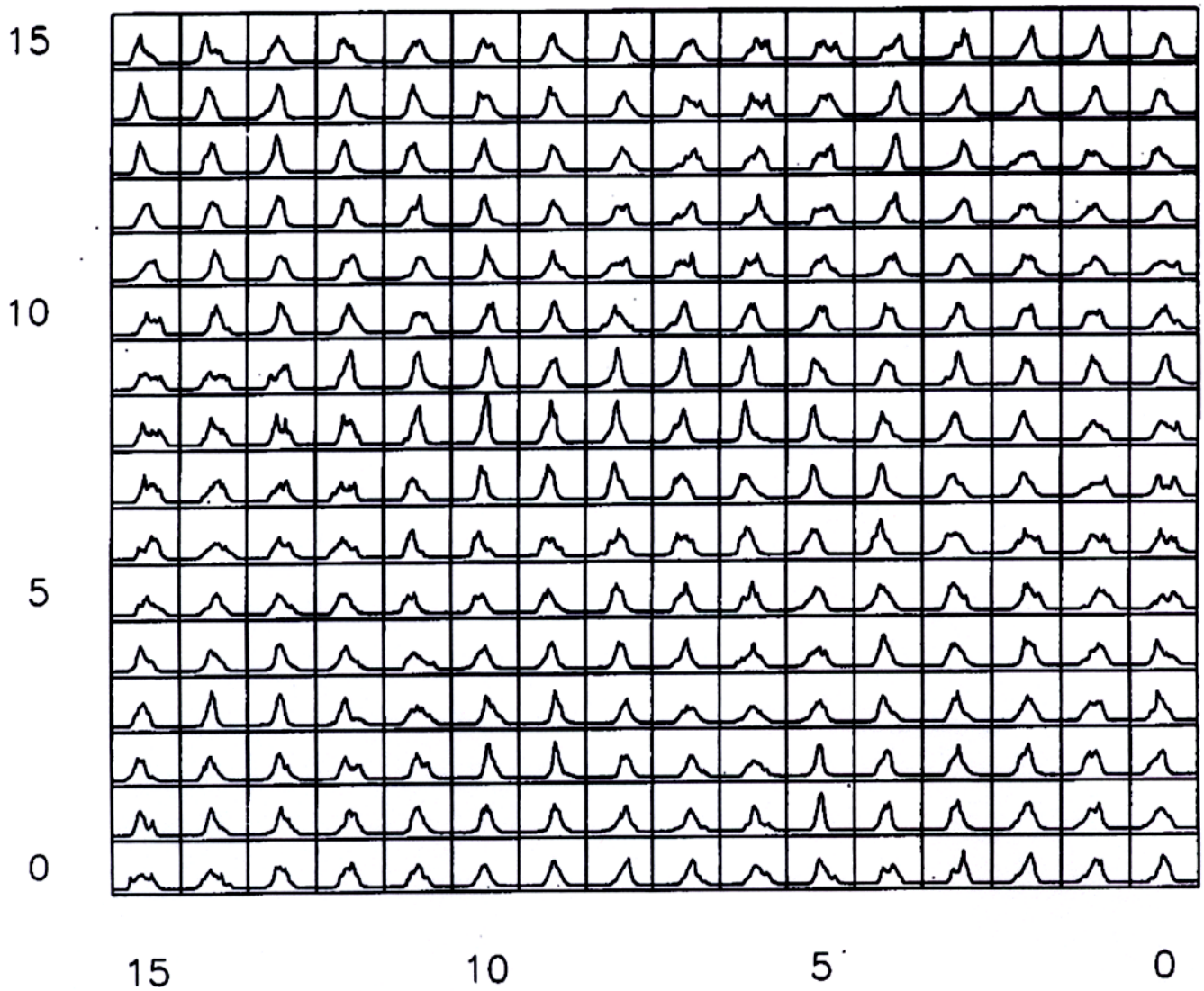

H[illegible] [illegible]titude Upsa Major cloud
$^{12}CO(2-1)$ from CSO.

2a

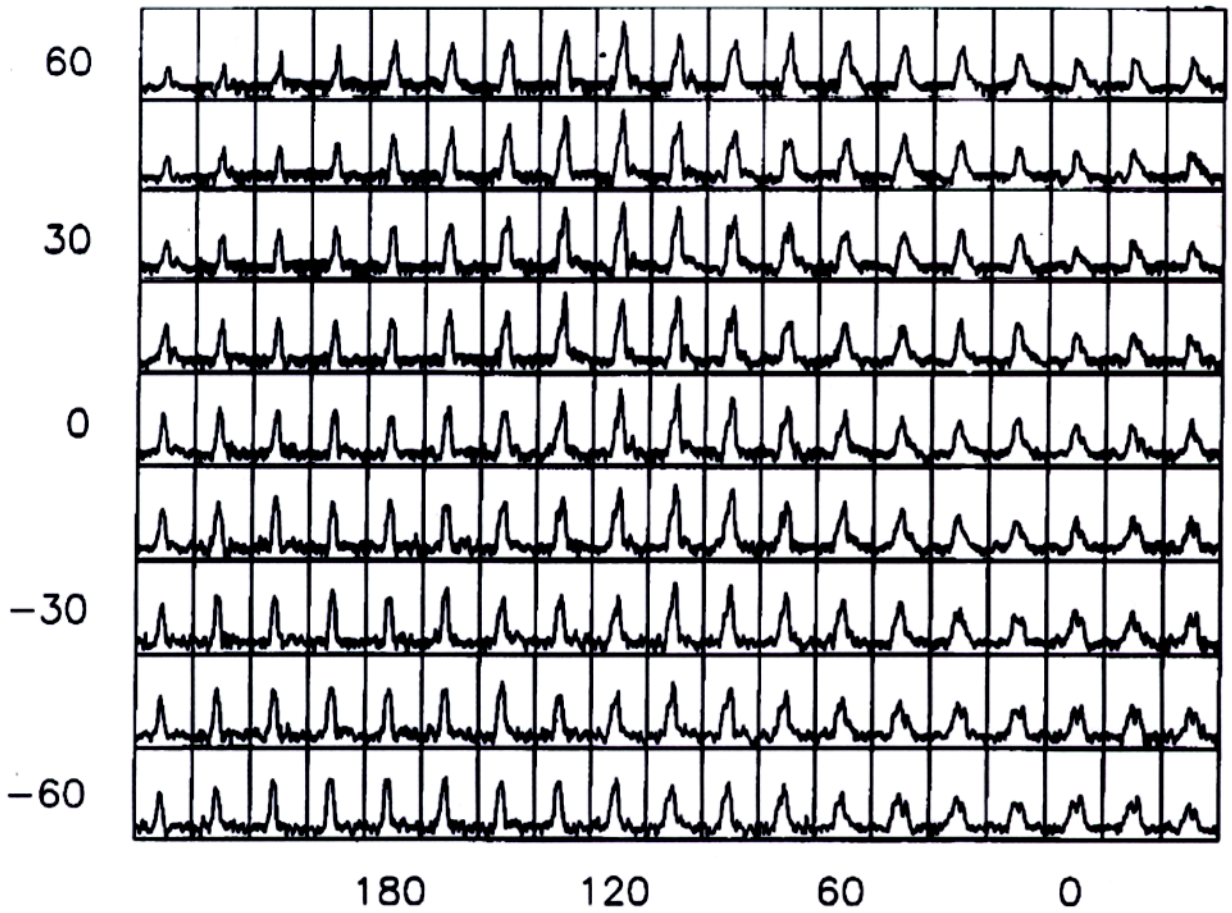

2b

subset

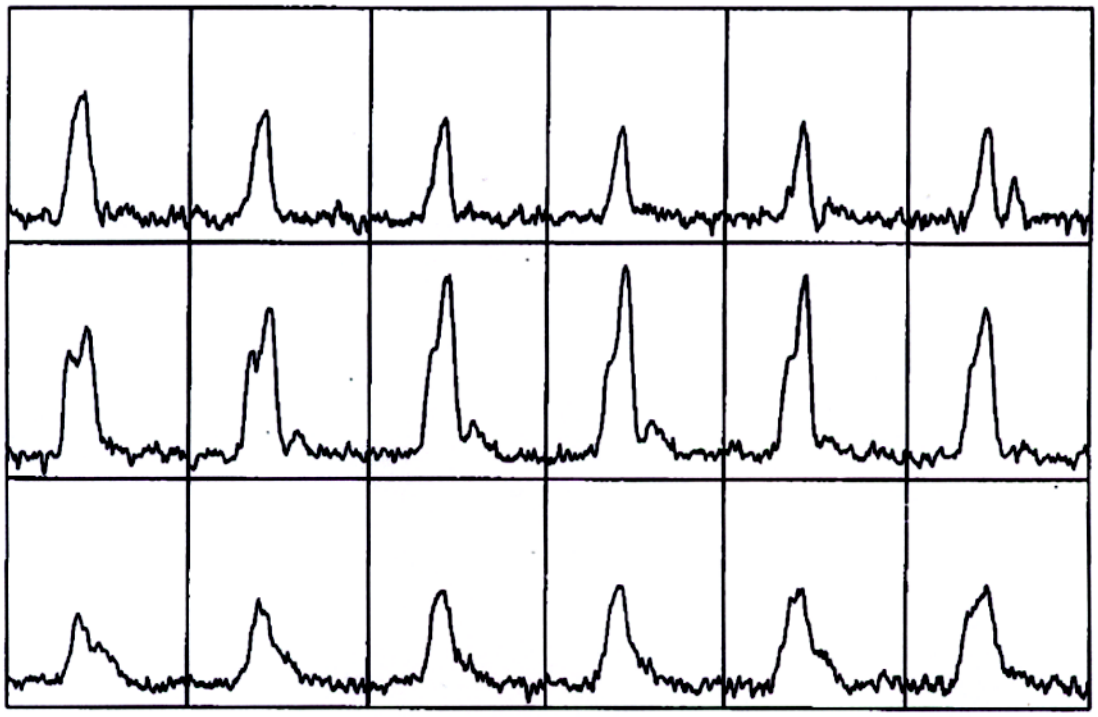

wings, skewness, multiple structures.

$T_{CO} \sim 10$; ^{13}CO shows same structure.

Barnard 1 ND_3 (1_0-0_0)

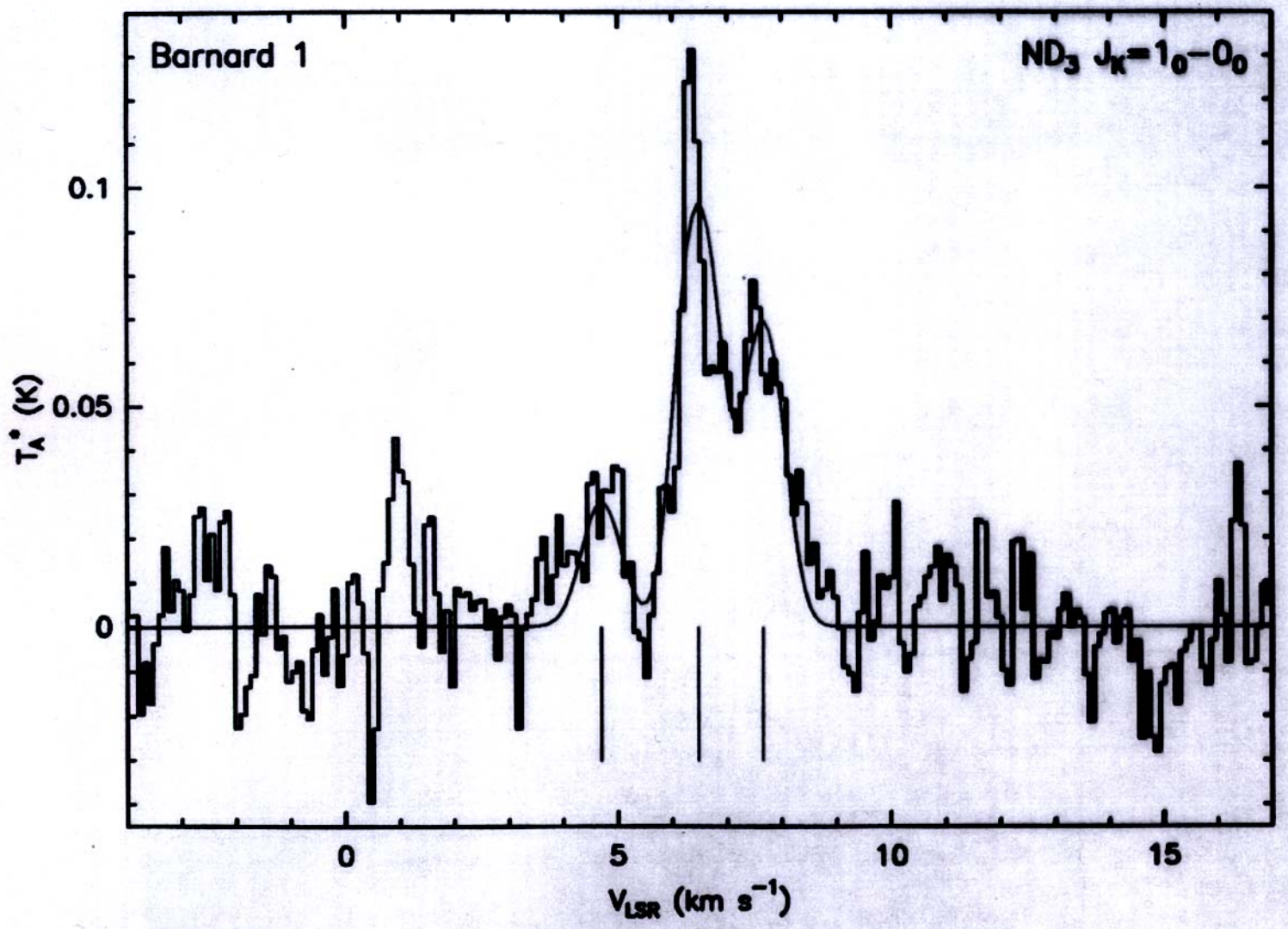

Barnard 1 DCO^+ (3-2)

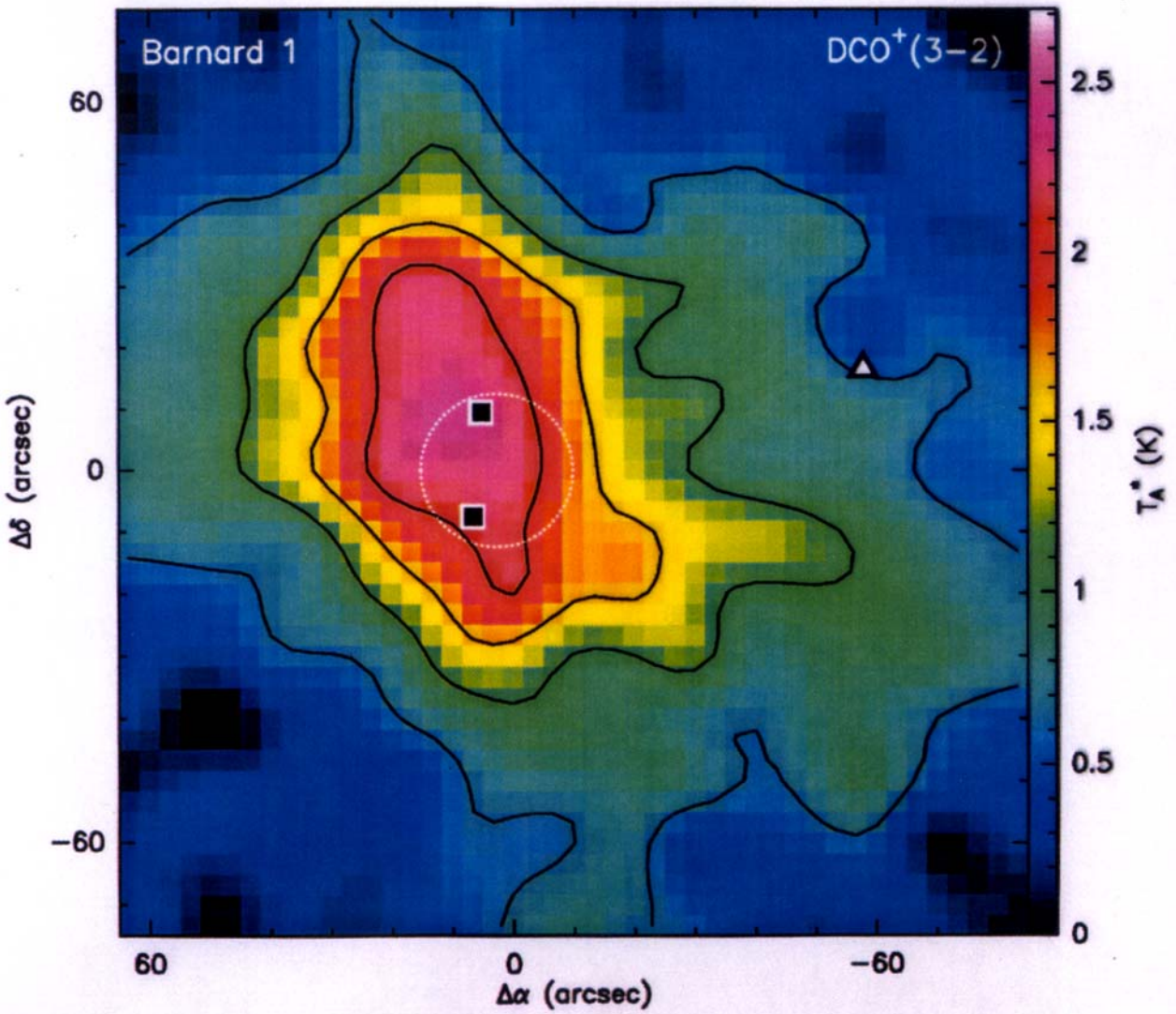

Submillimeter HCN Laser in IRC10216

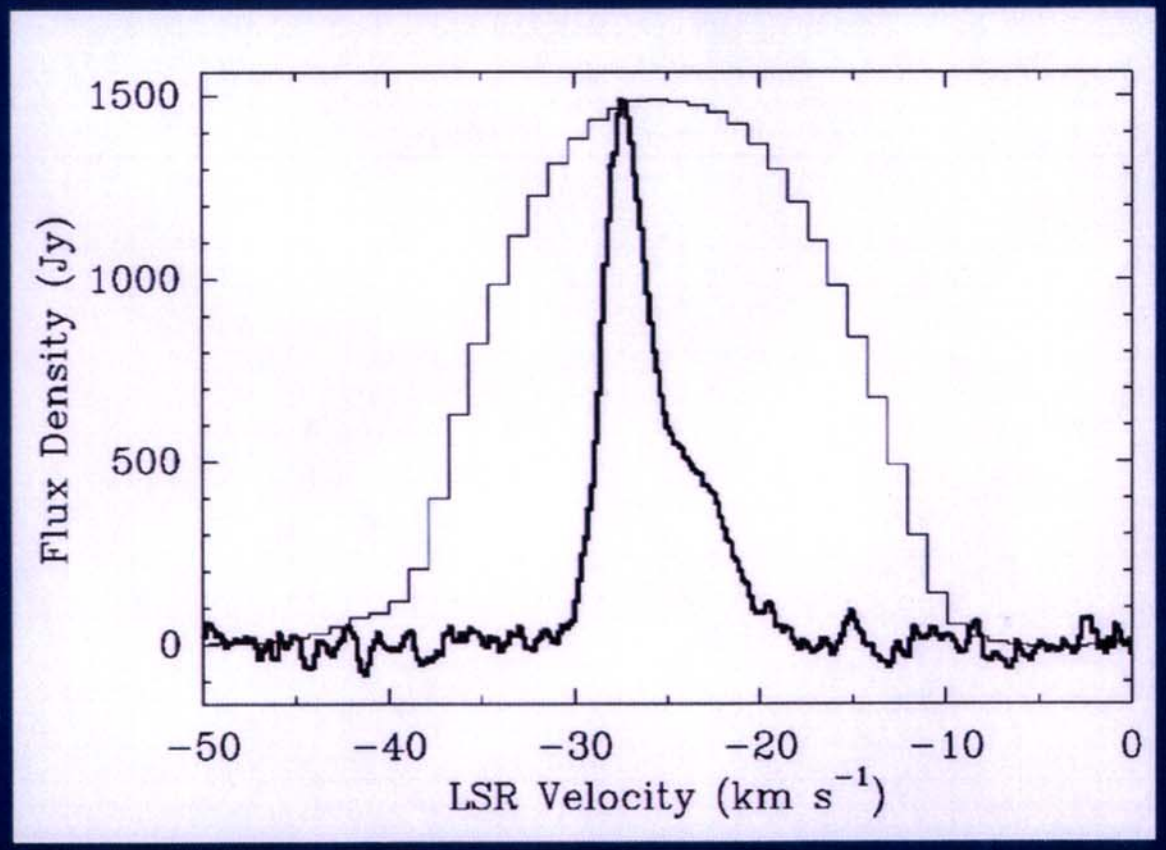

(805 GHz; Schilke et al., 2000)

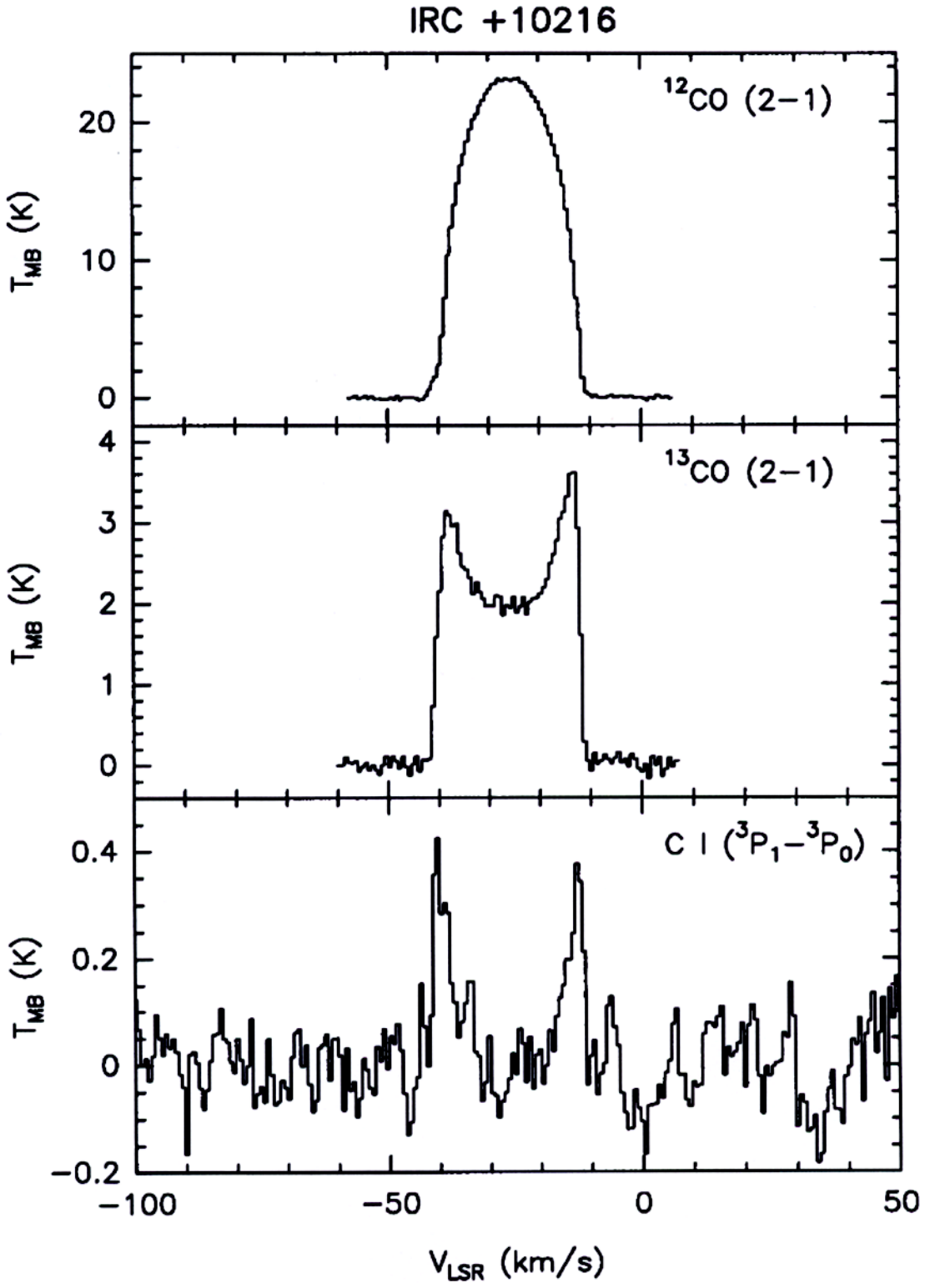
IRC +10216
^{12}CO (2−1)
^{13}CO (2−1)
C I ($^3P_1$−$^3P_0$)
T_{MB} (K)
V_{LSR} (km/s)
20
10
0
4
3
2
1
0.4
0.2
−0.2
−100
−50
0
50

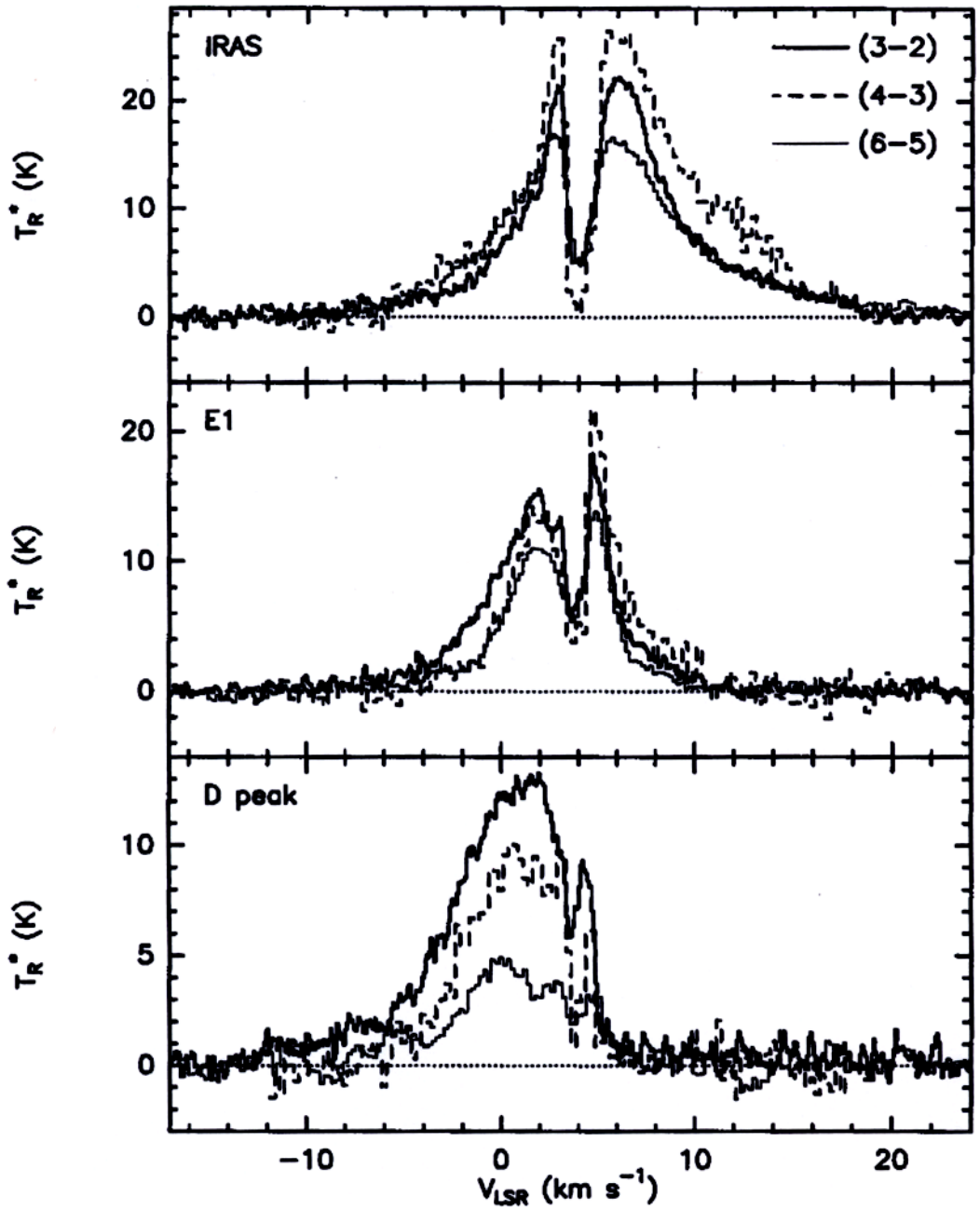
IRAS
(3–2)
(4–3)
(6–5)
E1
D peak
T_R^* (K)
V_{LSR} (km s^{-1})
20
10
0
5
−10
0
10
20

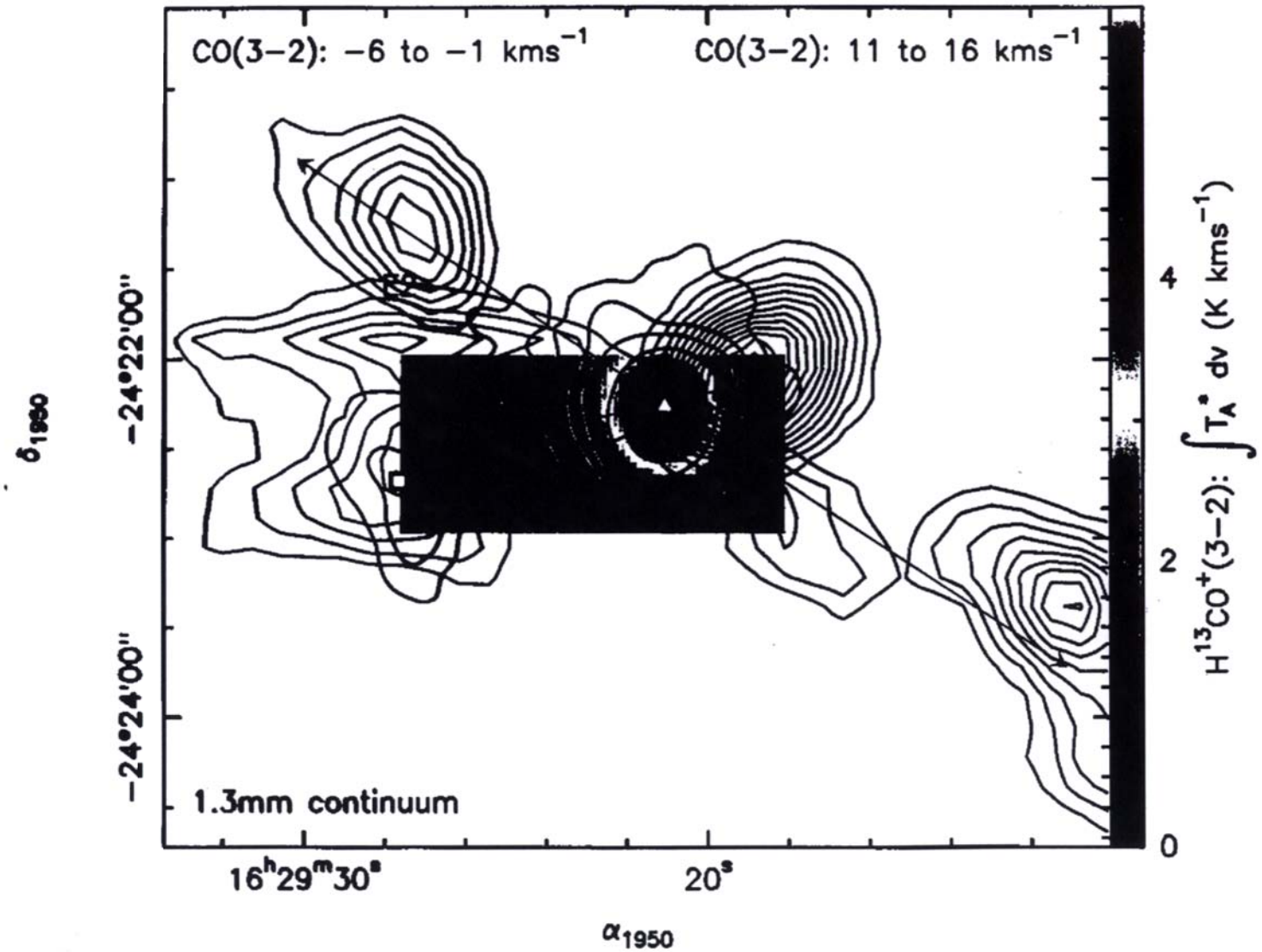
CO(3−2): −6 to −1 kms^{-1}
CO(3−2): 11 to 16 kms^{-1}
1.3mm continuum
−24°22'00"
−24°24'00"
δ_{1950}
16^{h}29^{m}30^s
20^s
α_{1950}
0
2
4
$H^{13}CO^+(3-2)$: $\int T_A^* dv$ (K kms^{-1})

Data

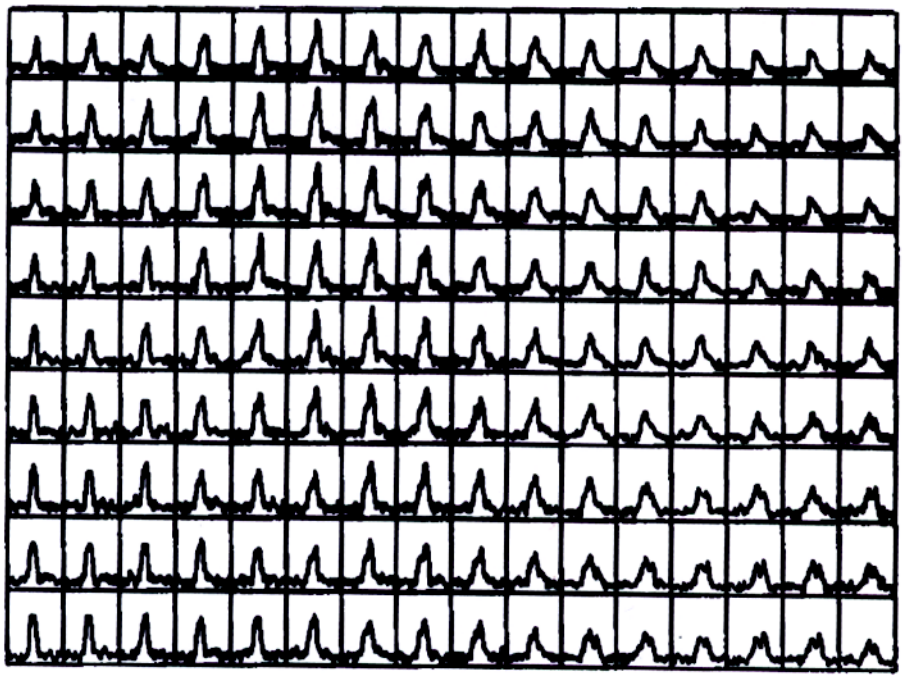

Simulation

Porter, Pouquet & Woodward + Falgarone, Phillips and Lis.

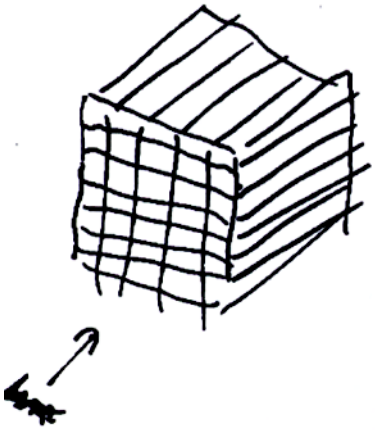

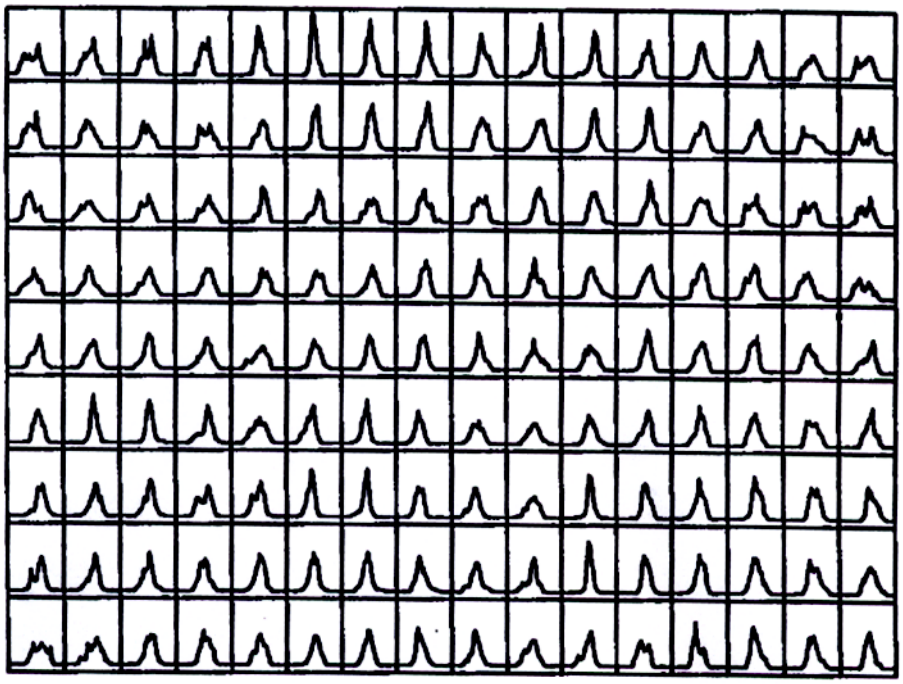

Figure IV7. (Top) ^{12}CO 2 – 1 spectra near the edge of a quiescent molecular cloud in Ursa Major. Note the diversity of the observed line shapes on the scale of ~ 0.02 pc. The spectra are often asymmetric, show broad wings and multiple velocity components. (Bottom) Simulated spectra based on the turbulent velocity field from the simulation of Porter *et al.* (1992). Note the close similarity of the model line shapes to those of the observed molecular spectra. These model spectra have been generated by us under the assumption of optically thin emission. Spike features are likely to be suppressed by opacity effects.

NGC1333 DCO^+ (3-2)

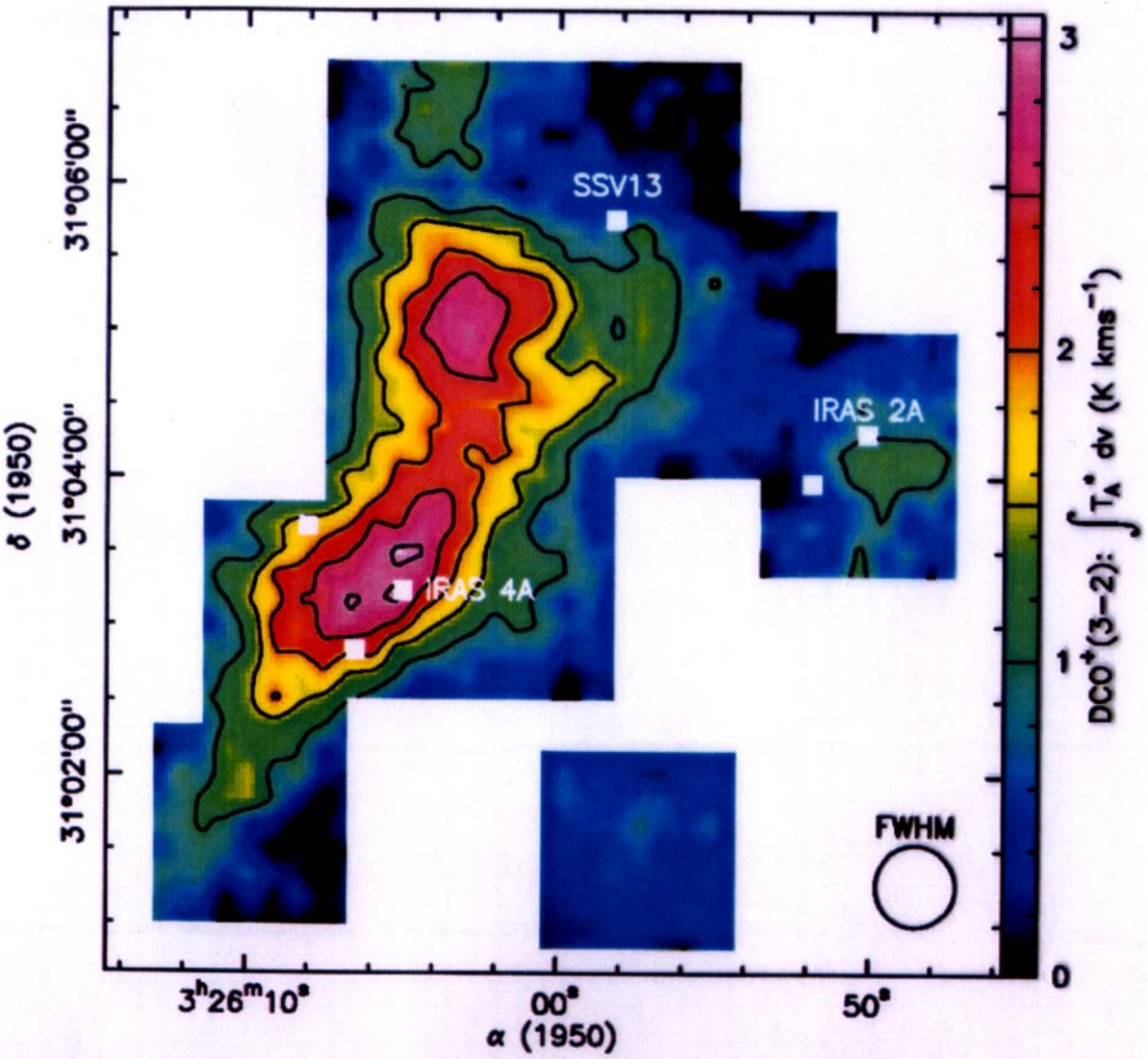

NGC1333 ND_3 (1_0-0_0)

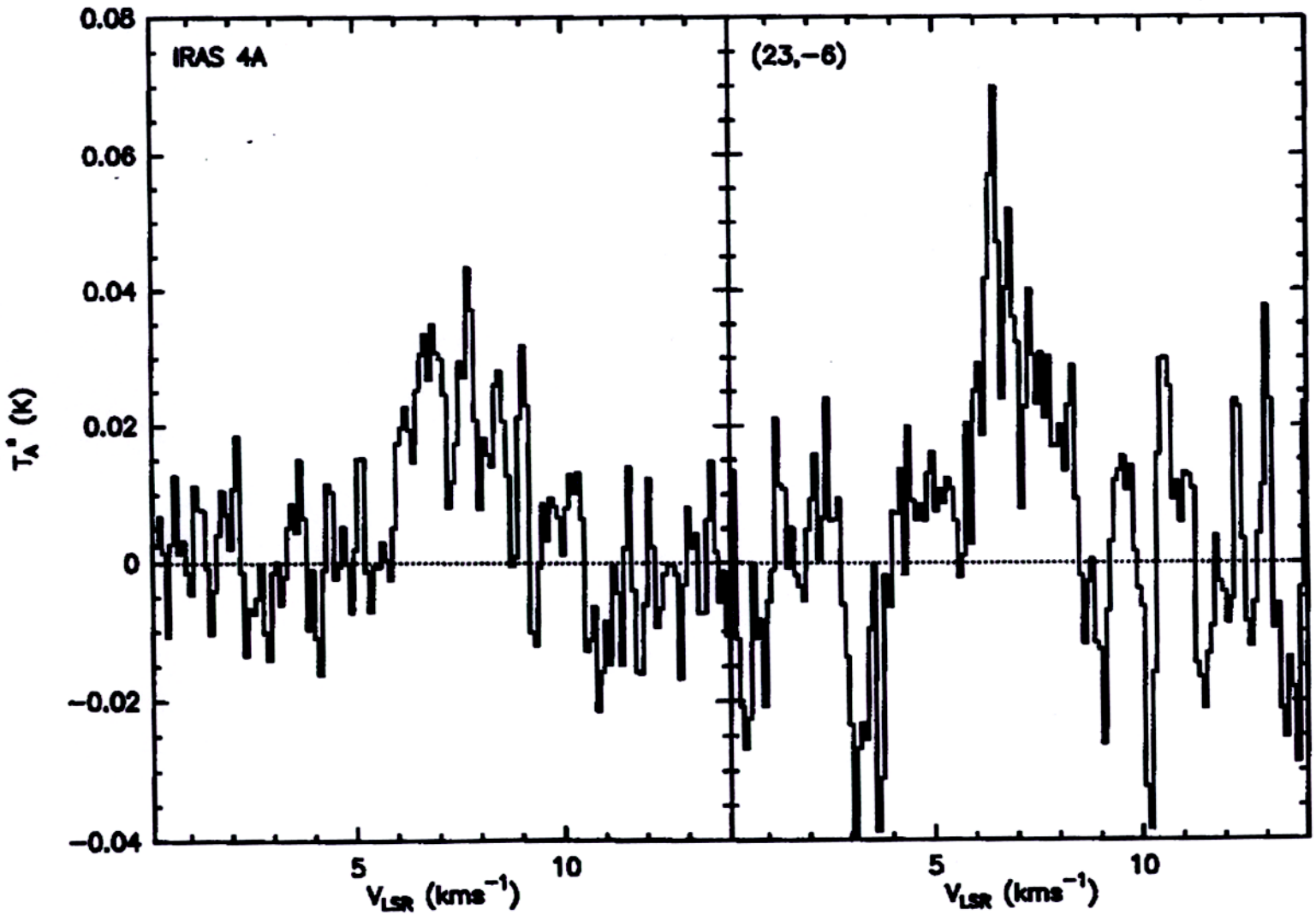

Figure I.3 ISO spectra from Fischer et al. 1999.

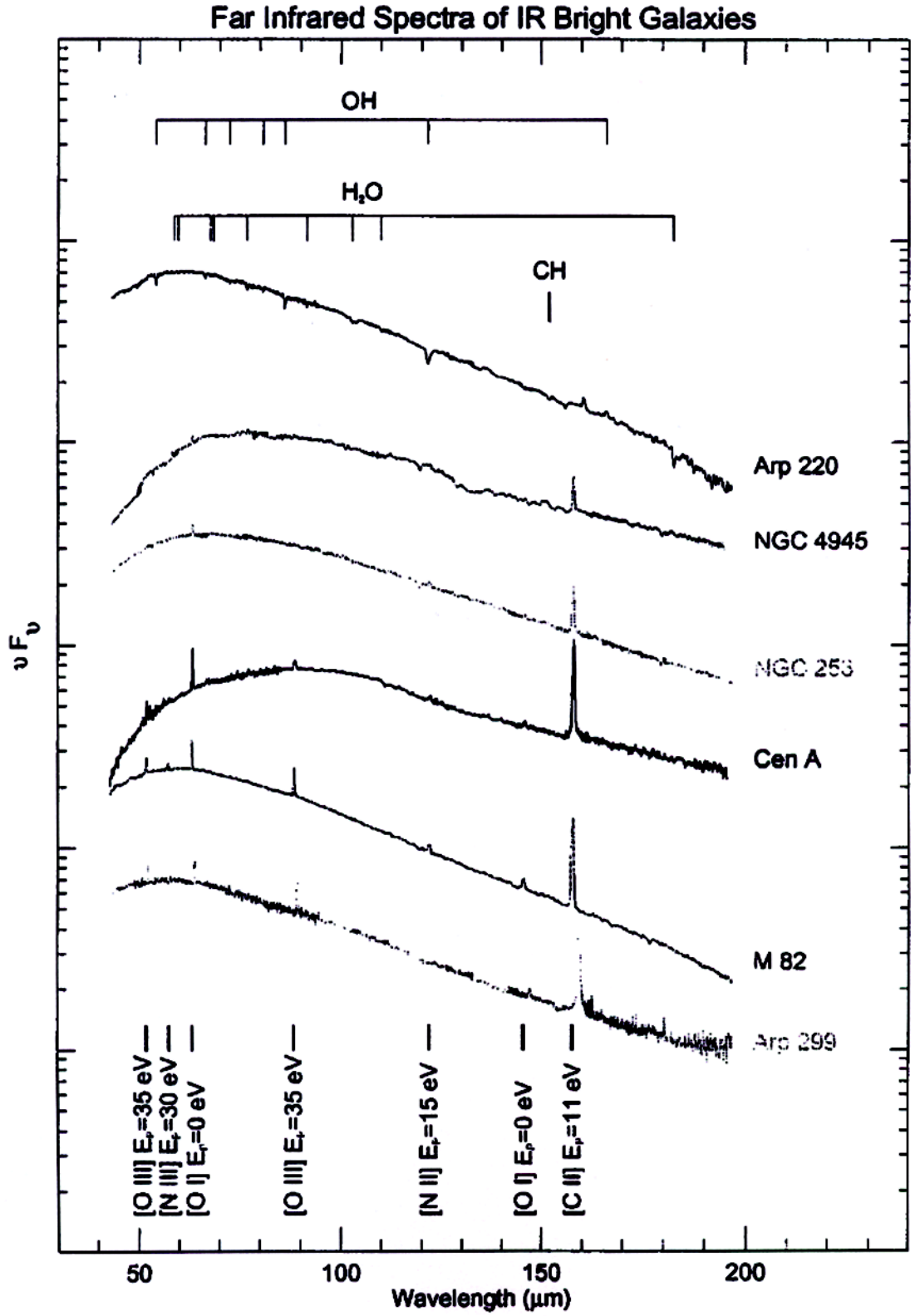

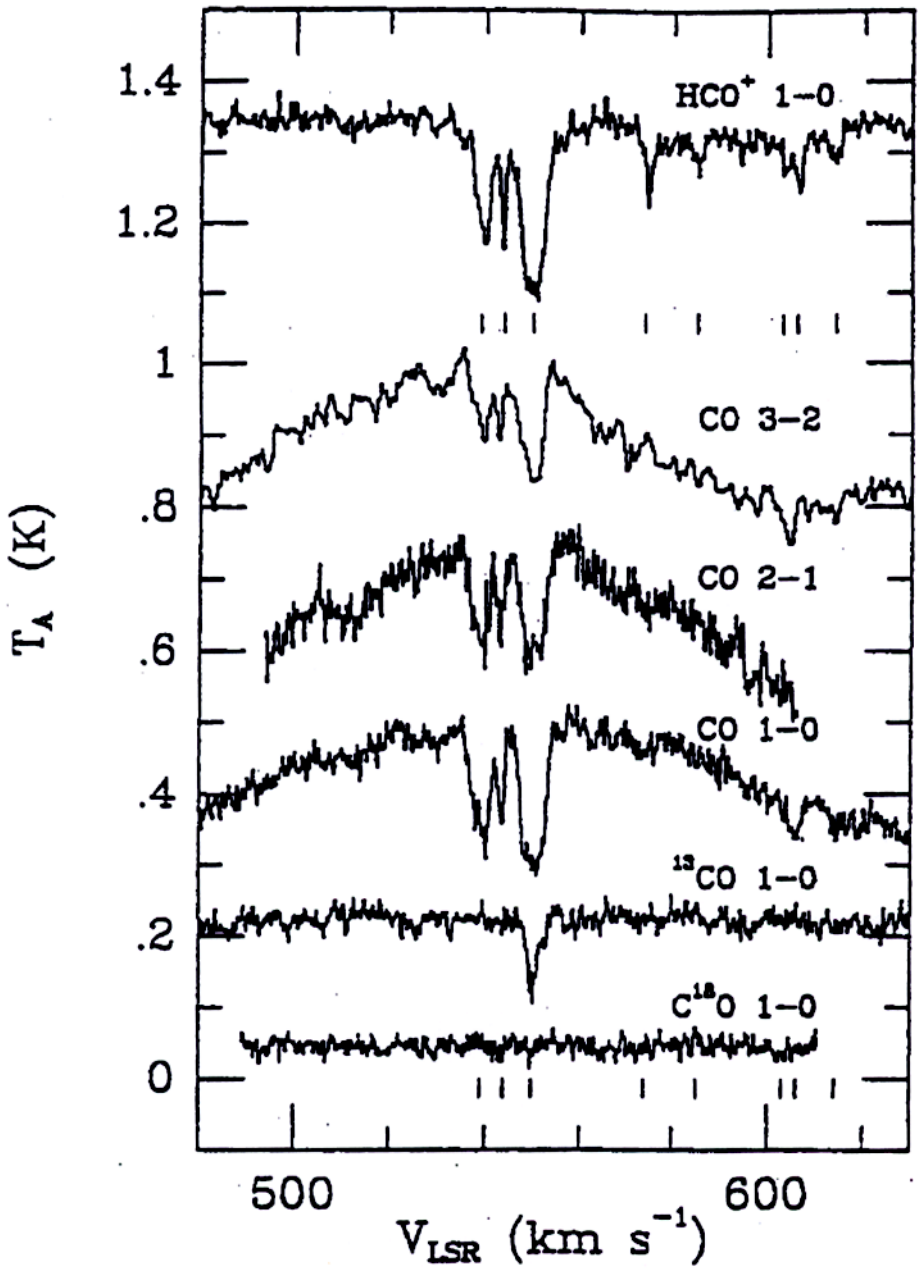

Fig. 2. High–resolution spectra of HCO^+ 1–0, ^{12}CO 3–2, 2–1 and 1–0, ^{13}CO 1–0 and $C^{18}O$ 1–0 toward the nucleus of Centaurus A. The spectra have been shifted in T_A^* by +1.05, +0.4, +0.25, 0.0, -0.05 K and -0.20 K, and have velocity resolutions of 0.29, 0.9, 0.23, 0.23, 0.23 and 0.23 km s^{-1}, respectively. Note the numerous absorption components in the HCO^+ spectrum at red–shifted velocities.

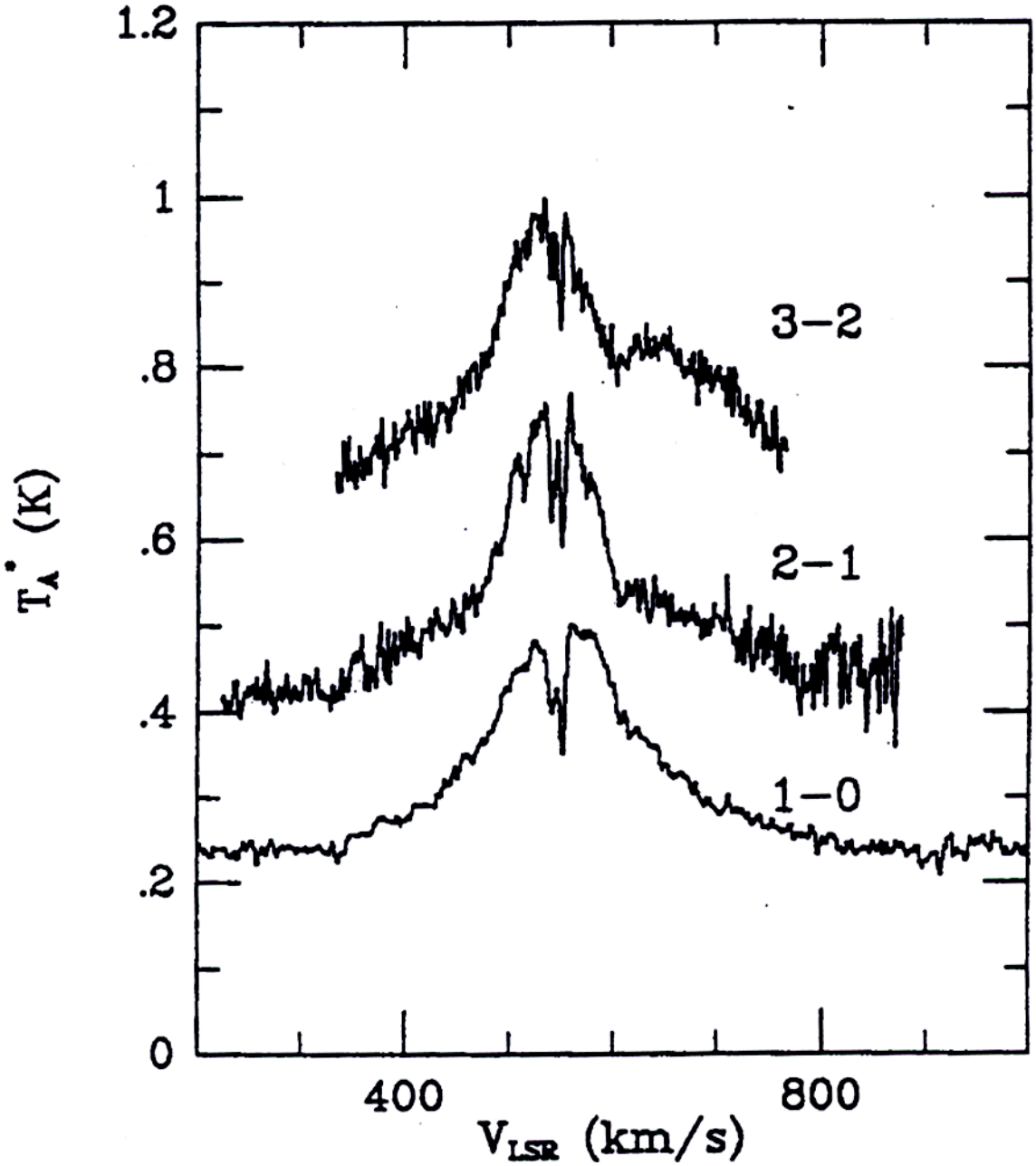

Fig. 1. ^{12}CO 1–0, 2–1 and 3–2 spectra toward the nucleus of Centaurus A, smoothed to 2.8, 0.9 and 0.9 km s^{-1} resolution. The 2–1 and 3–2 spectra have been shifted in T_A^* by +0.25 and +0.45 K respectively.

Rel. Offset (arcmin)

-2.70 1.32

-2.25 1.10

-1.80 0.88

-1.35 0.66

-1.12 0.55

-0.90 0.44

-0.67 0.33

-0.45 0.22

-0.22 0.11

0.0 0.0

0.22 -0.11

0.45 -0.22

0.67 -0.33

0.90 -0.44

1.12 -0.55

1.35 -0.66

1.80 -0.88

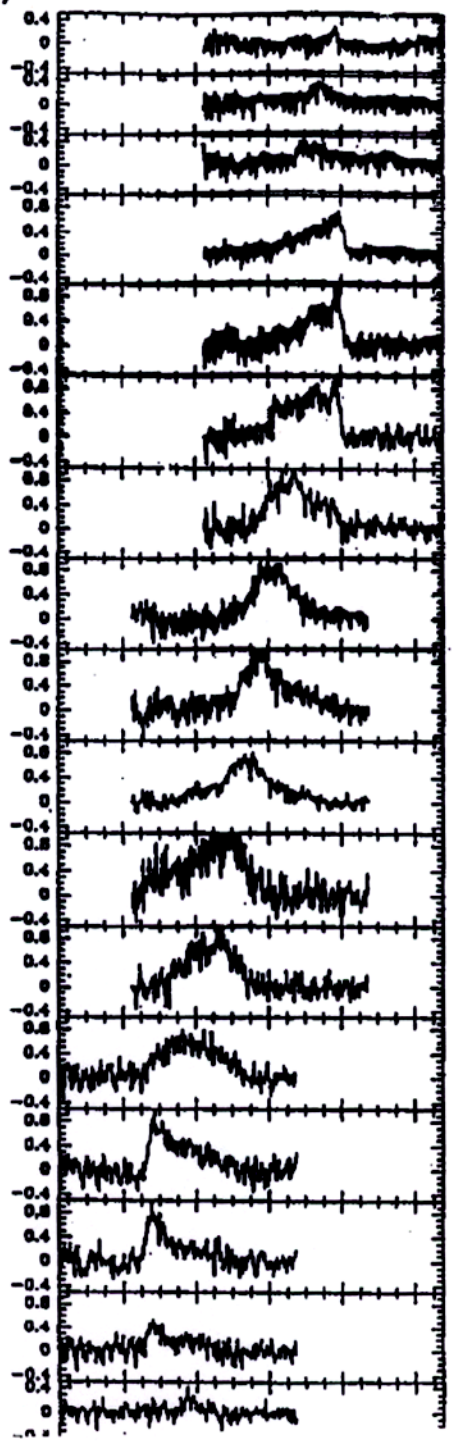

Predicted Spectra of Glycine

THZ Spectra of Glycine Conformers

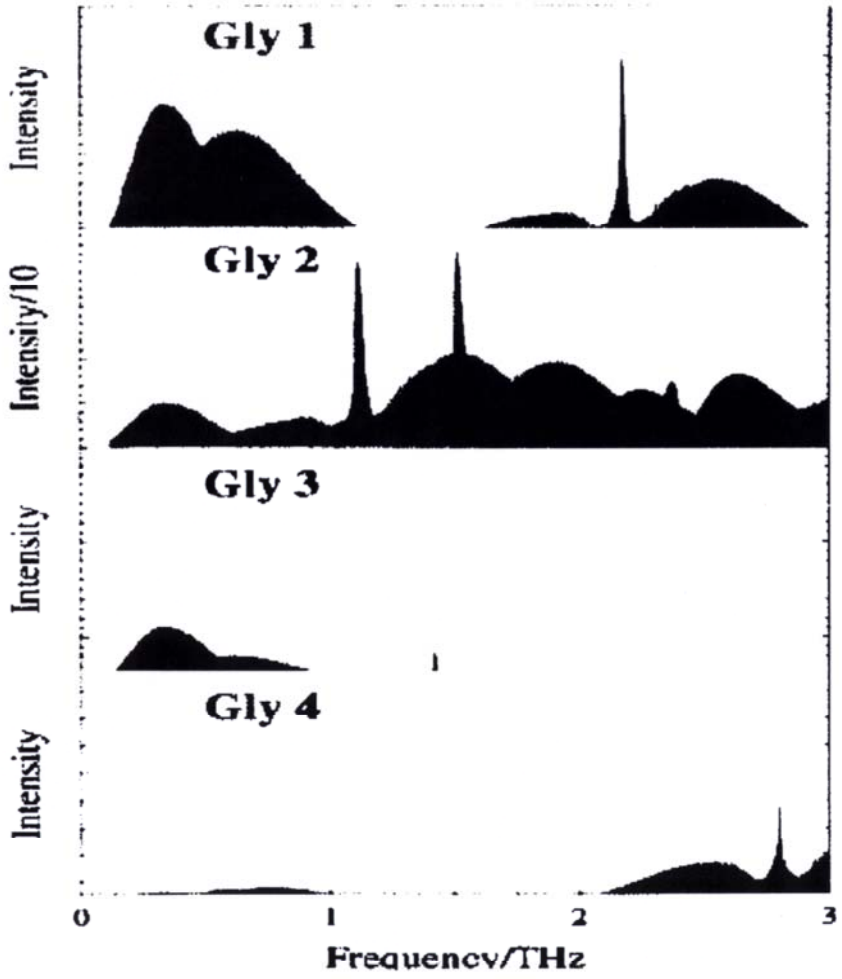

Lowest Bending Modes of Linear Carbon Clusters

and HIFI Receiver Bands

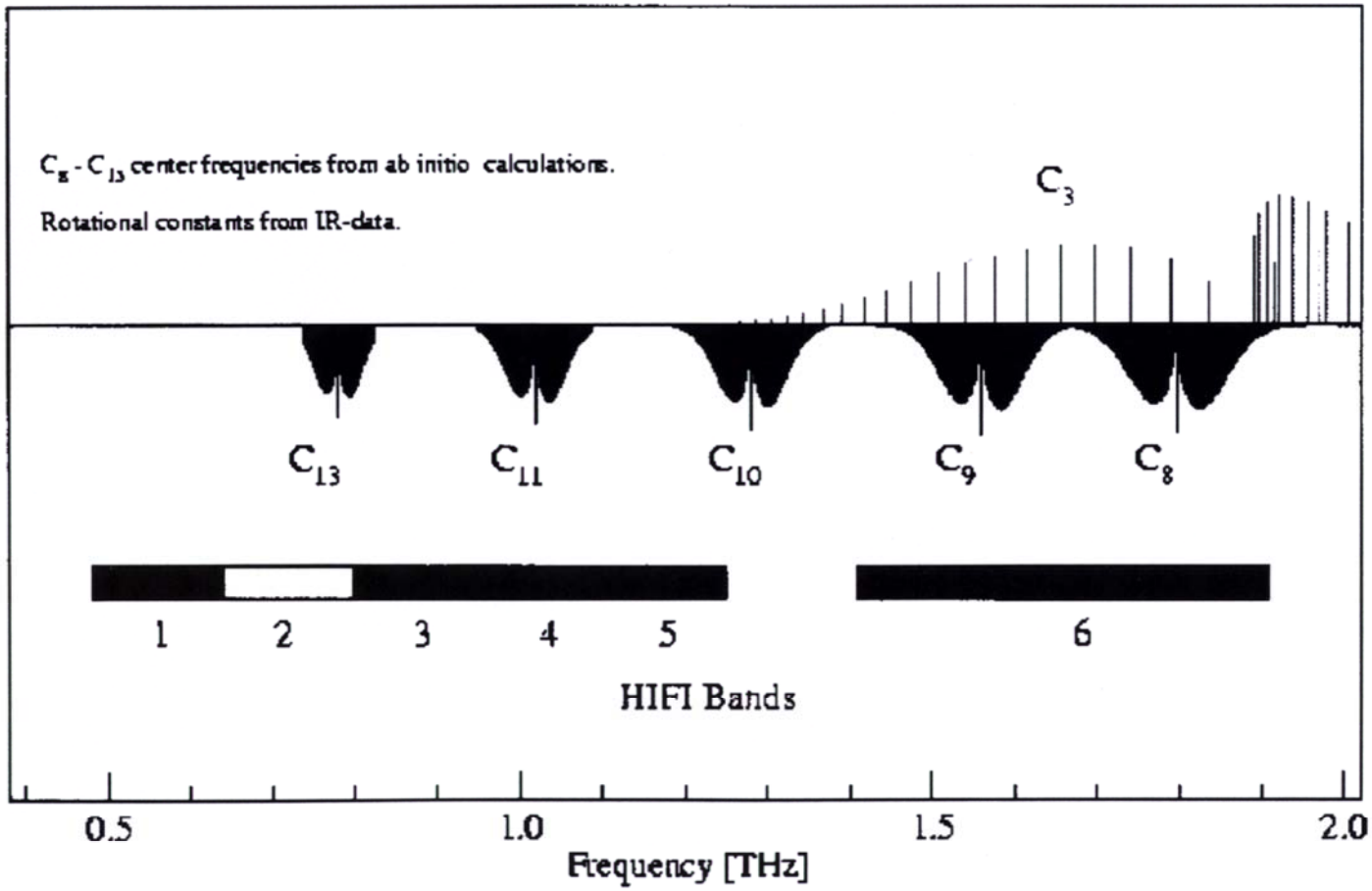

L1689N ND_3 (1_0-0_0)

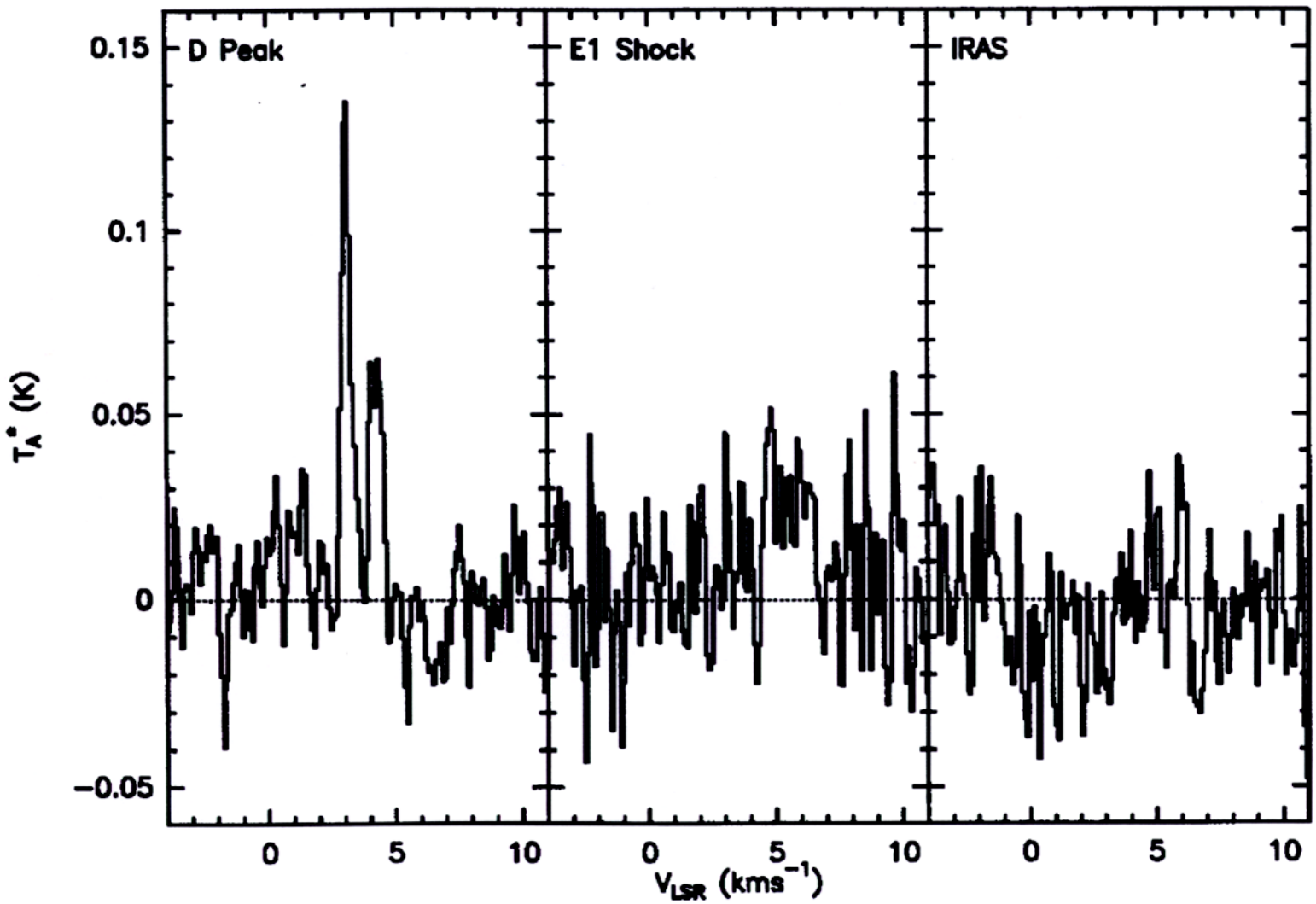

L1689N Deuterium Peak

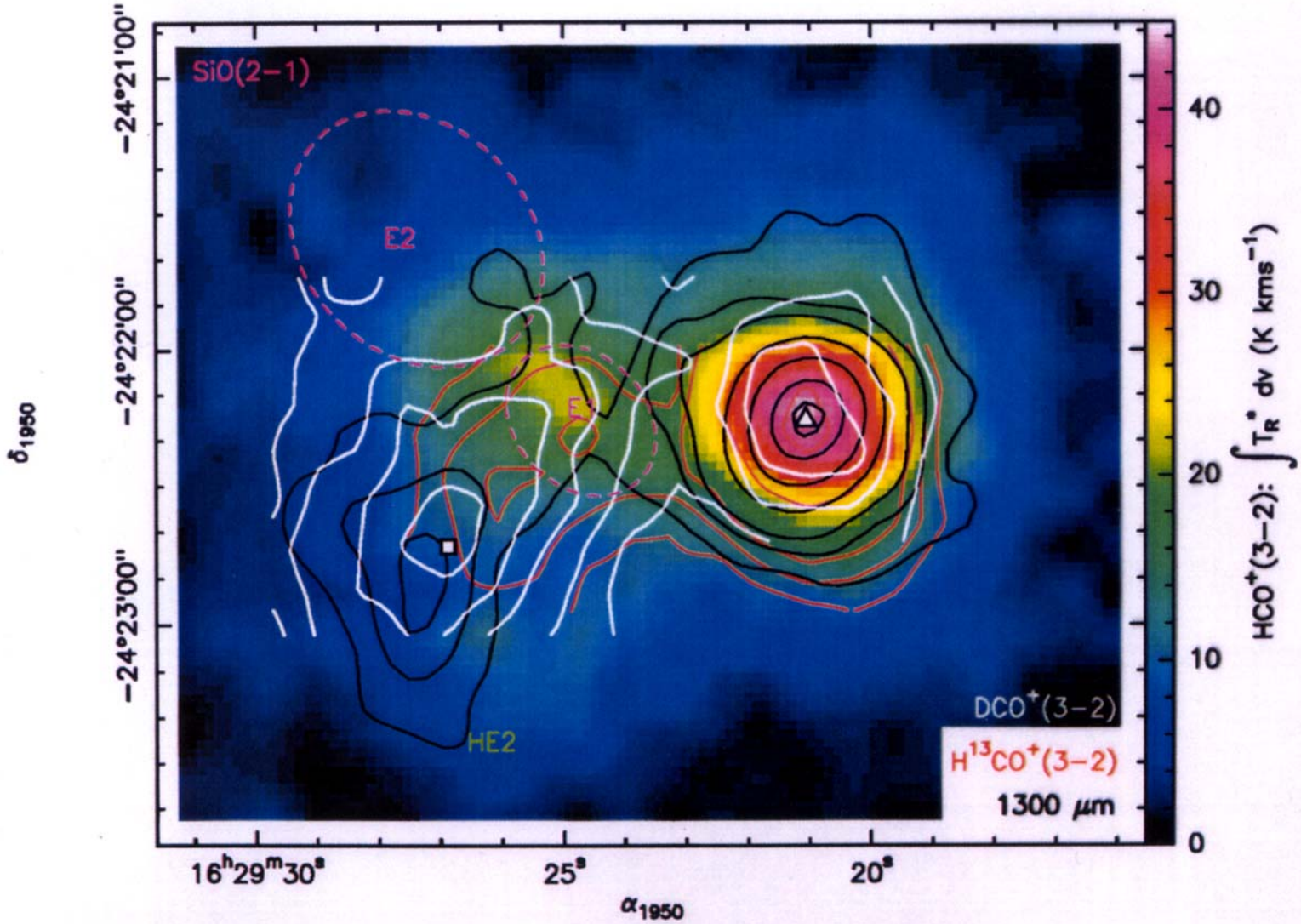

from Pierre Cox

ISO/LWS Spectrum of
The Ultraluminous Galaxy ARP 220

Fischer et al. (in prep)

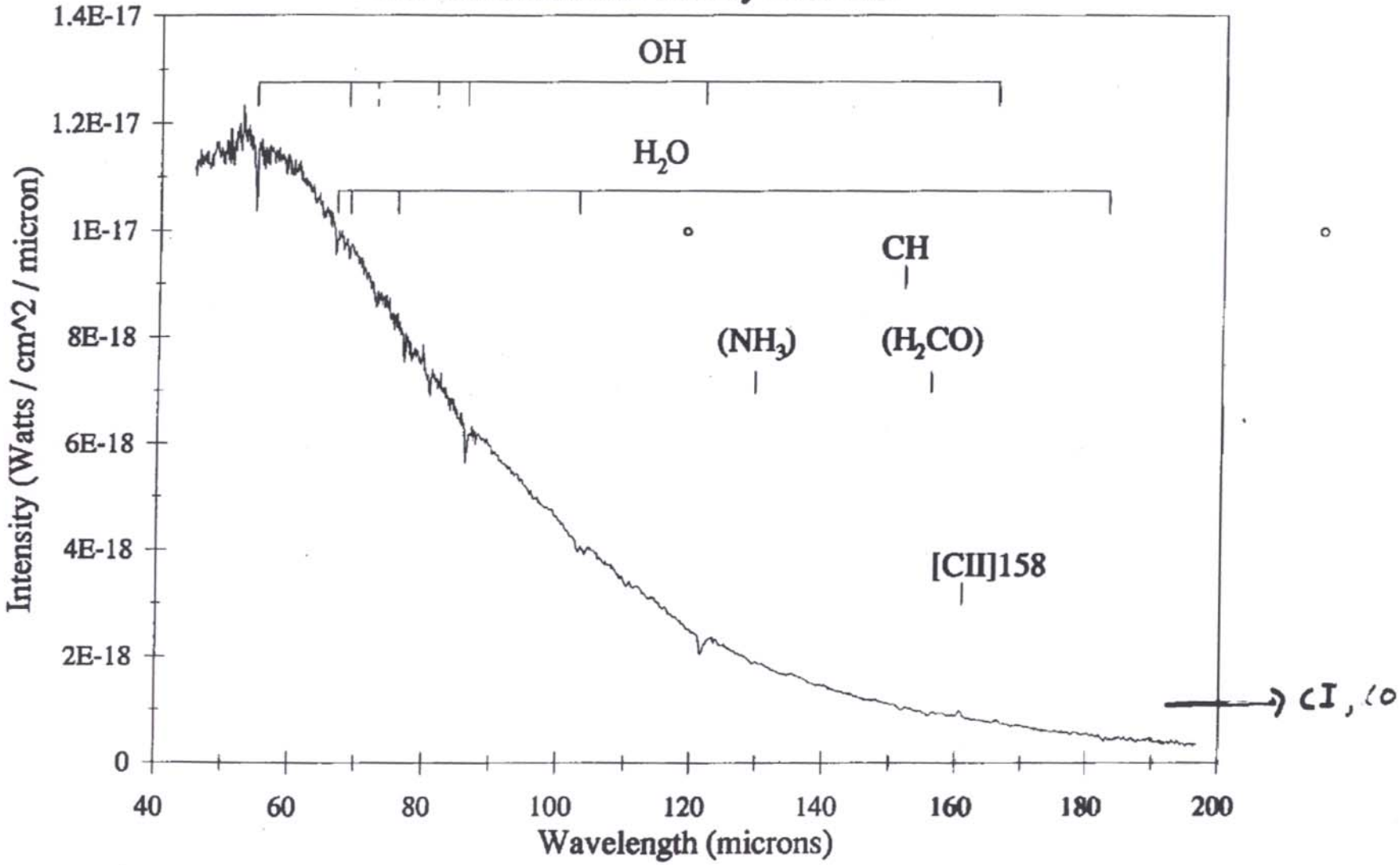

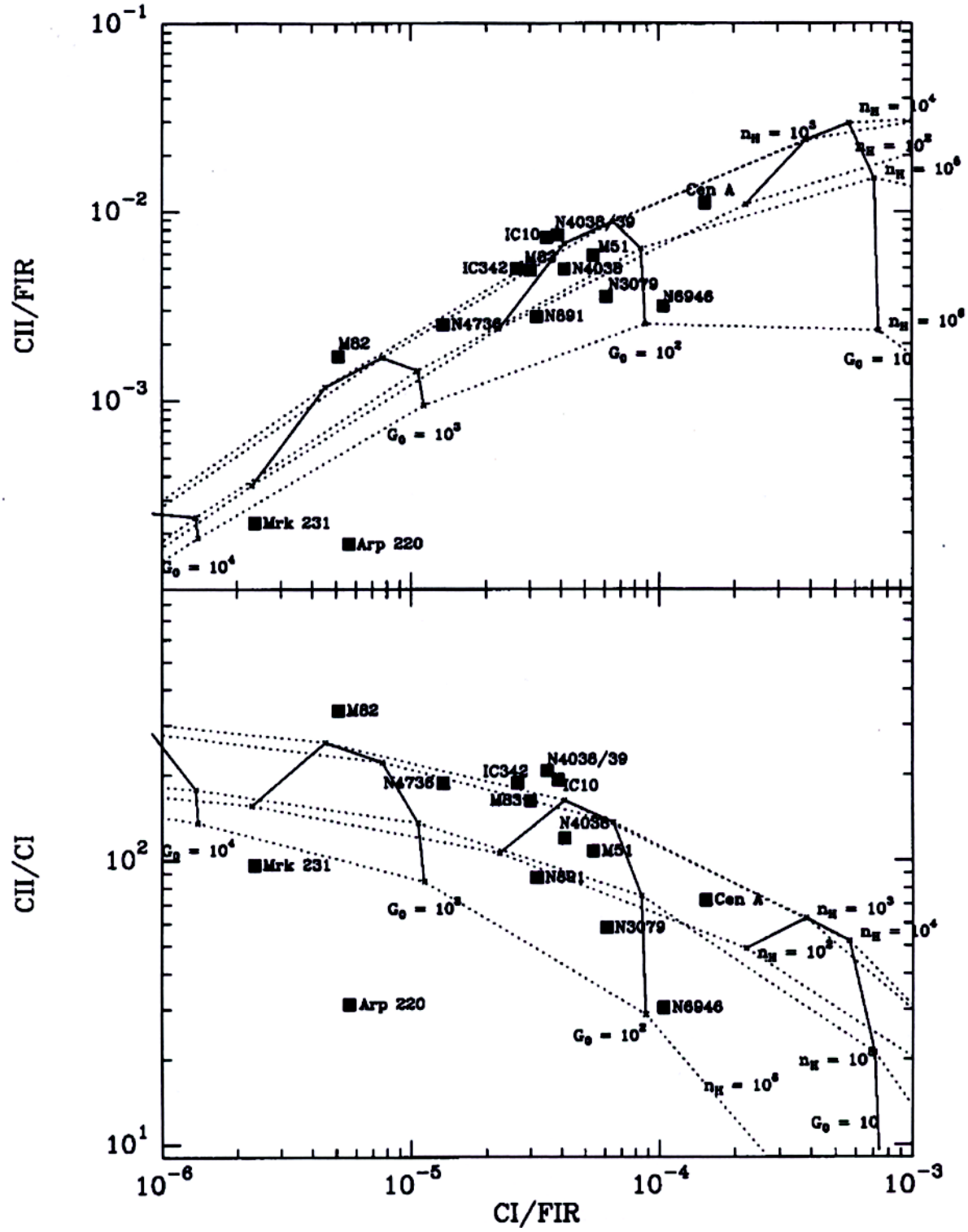
CII/FIR
CII/CI
CI/FIR
10^{-1}
10^{-2}
10^{-3}
10^{2}
10^{1}
10^{-6}
10^{-5}
10^{-4}
10^{-3}
Cen A
N4038/39
IC10
M51
M83
IC342
N4038
N3079
N6946
N4736
N891
M82
Mrk 231
Arp 220
$G_0 = 10^4$
$G_0 = 10^3$
$G_0 = 10^2$
$G_0 = 10$
$n_H = 10^4$
$n_H = 10^3$
$n_H = 10^2$
$n_H = 10^1$
$n_H = 10^0$

Observations of THz lines in Extra Solar Planetary Atmospheres

E.g. H_2O (111-000) at ~ 1 THz

- One 10 m telescope, beam = 1.2 $\lambda/D \approx 7''$

Planet at 1 pc, dia $\approx 10^{-4}''$ (Earthlike)
$\approx 10^{-3}''$ (Jupiterlike)

Beam dilution (B) $\approx 2 \times 10^{-10}$ (Earth)
$\approx 2 \times 10^{-8}$ (Jupiter)

Suppose – H_2O feature 100 K (T_s)
– $T_{Rx} = h\nu/k = 50$ K
– Resolution ≈ (30 MHz)

– Integration time = 1 yr

$$S/N \approx \frac{T_s}{T_{Rx}} \; [3 \times 10^7 \times 3 \times 10^7]^{1/2} \times B \approx 10^{-2} \text{ (Earth)}$$
$$\approx 1 \text{ (Jupiter)}$$

- Interferometer (ALMA in Space)

60 x 10m S/N ≈ 0.6 (Earth)

S/N ≈ 60 (Jupiter)

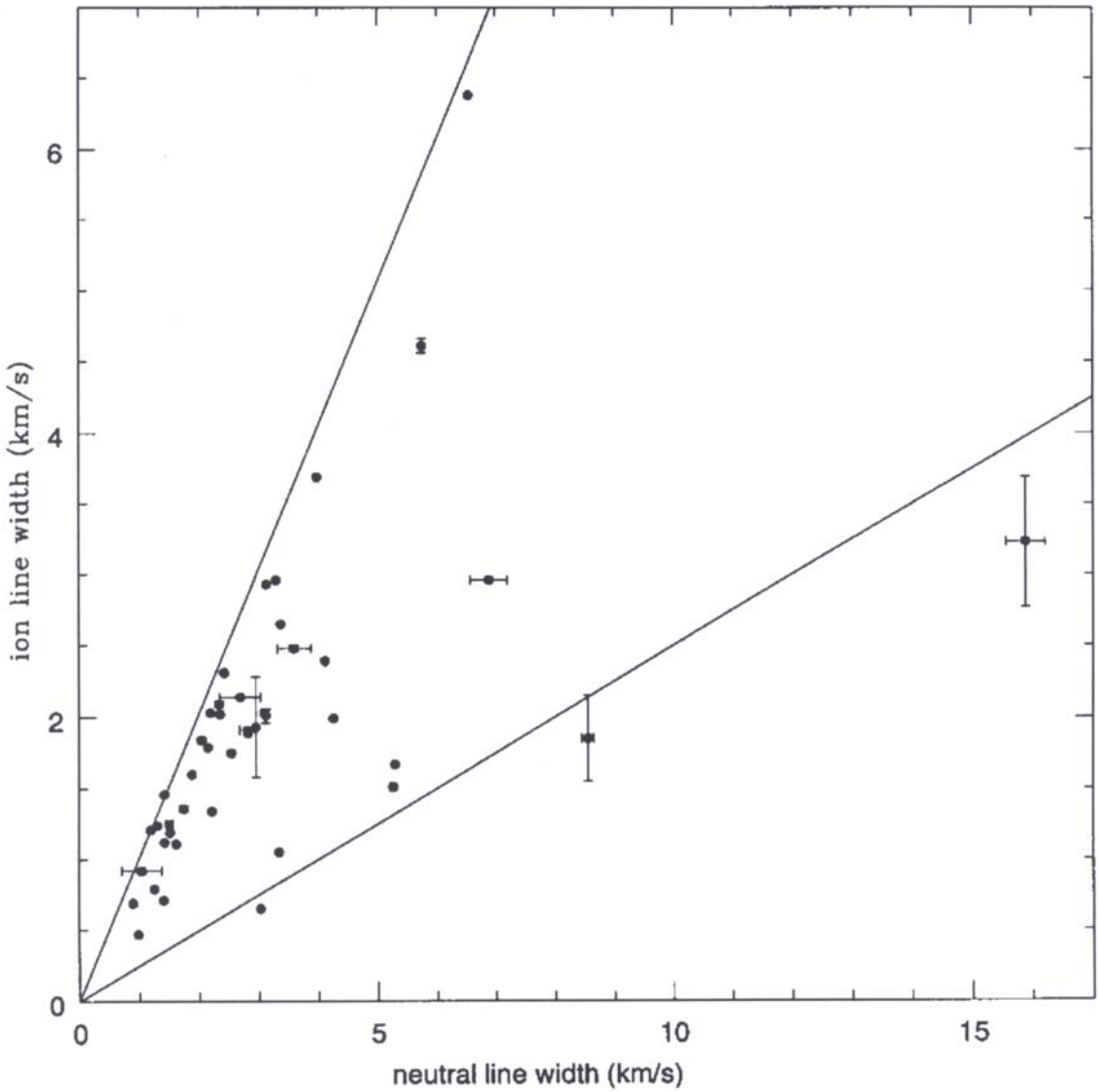

Fig. 13.— Plot of ion vs neutral line widths. The two straight lines show the limits discussed above (line ratios of $\simeq 1$ and $\simeq 0.25$).

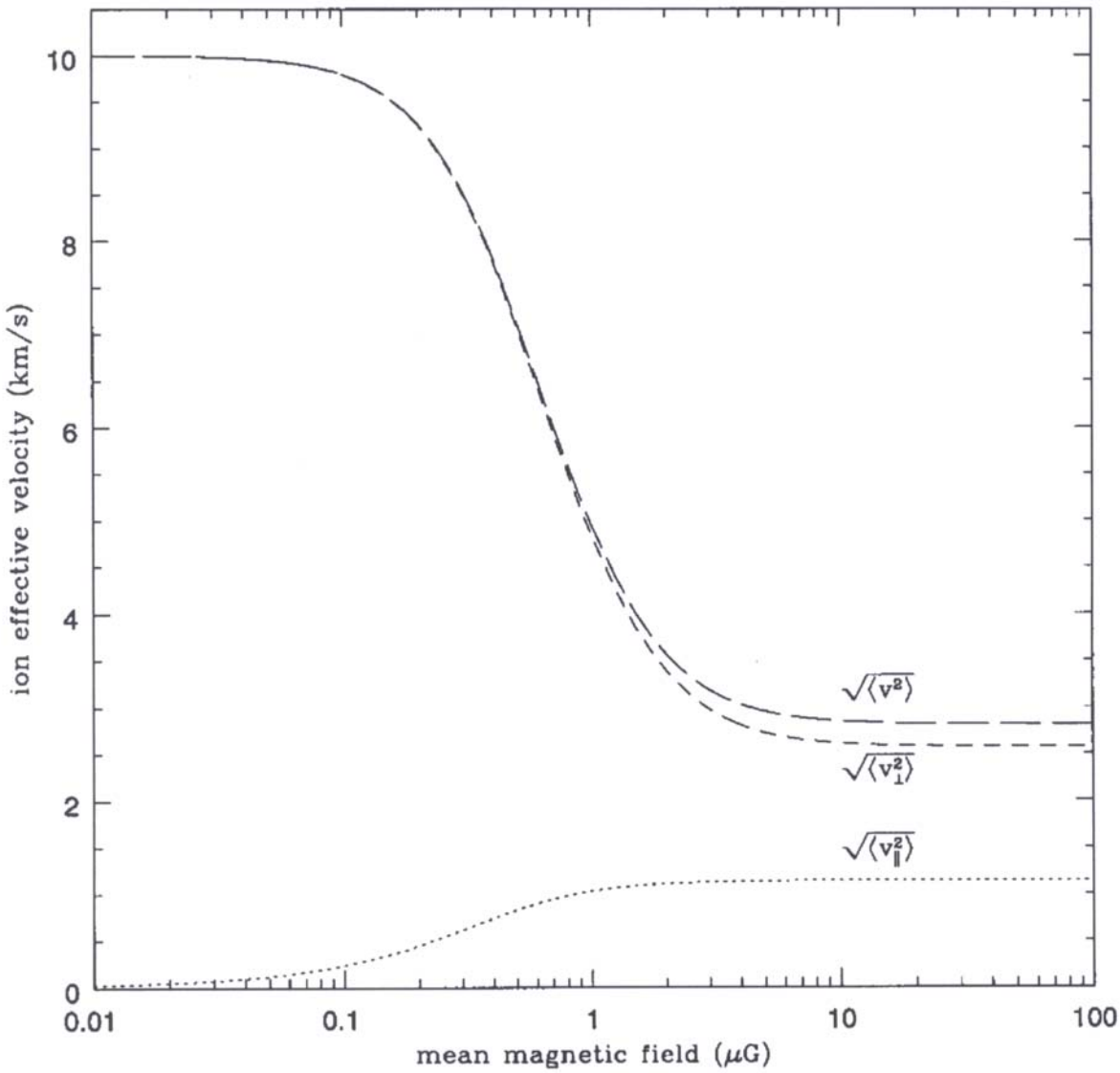

Fig. 3.— Ion effective velocity ($\left\langle \mathbf{v}_\parallel^2 \right\rangle^{\frac{1}{2}}$, $\langle \mathbf{v}_\perp^2 \rangle^{\frac{1}{2}}$ and $\langle \mathbf{v}^2 \rangle^{\frac{1}{2}}$) as a function of the mean magnetic field strength when $\mathbf{v}_\parallel^n = 0$, $|\mathbf{v}_\perp^n| = 10$ km/s, $n = 10^6$ cm^{-3} and $A_i = 29$.

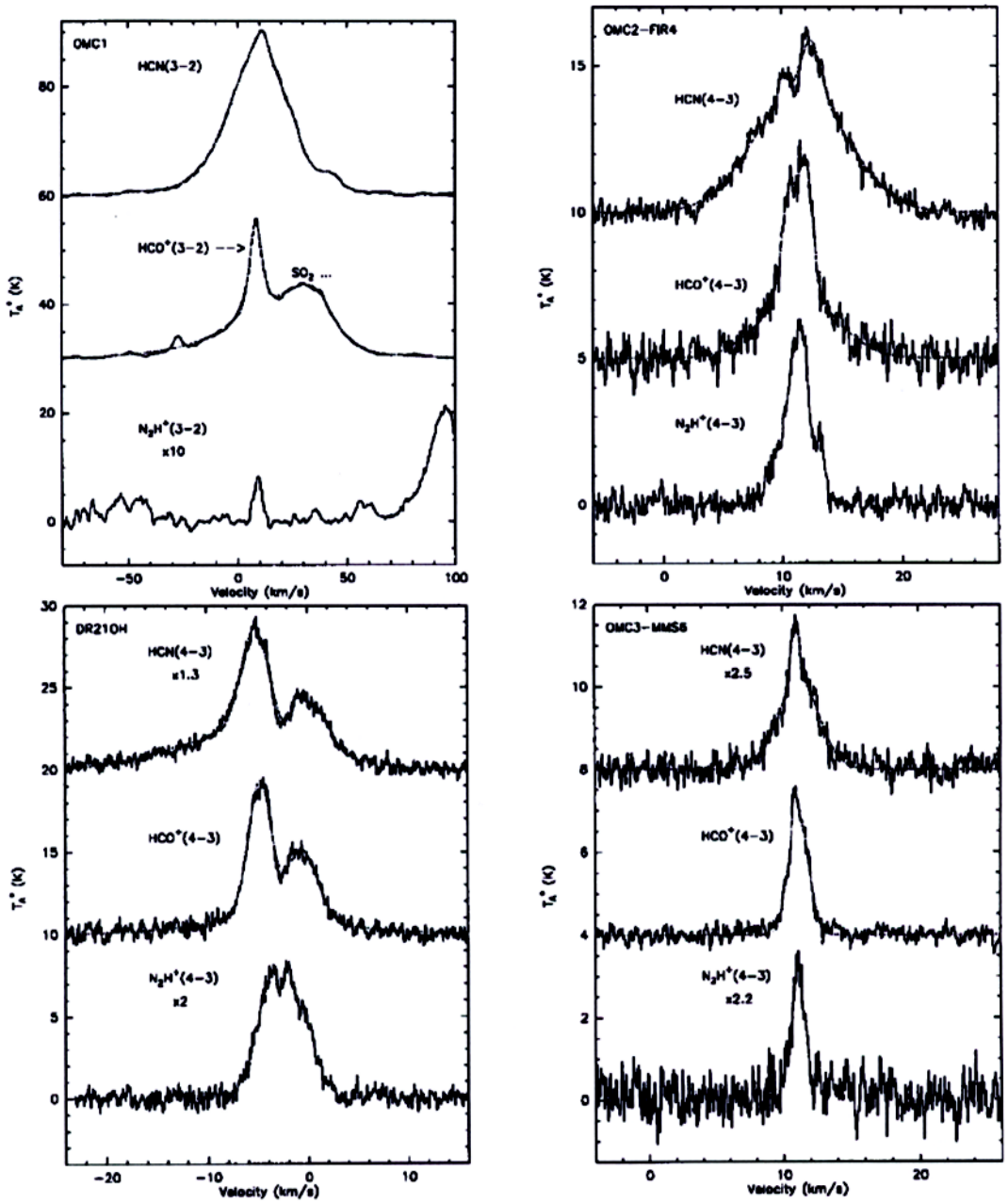

Fig. 6.— HCN (top), HCO^+(middle) and N_2H^+ (bottom) observations at the position of peak intensity of (clockwise starting from top left): OMC1, OMC2-FIR4, OMC3-MMS6 and DR21OH. The bump at $\sim$ 30 km/s in the middle spectrum of OMC1 is a contamination from other species (SO_2, $^{13}CH_3CN$, ...).

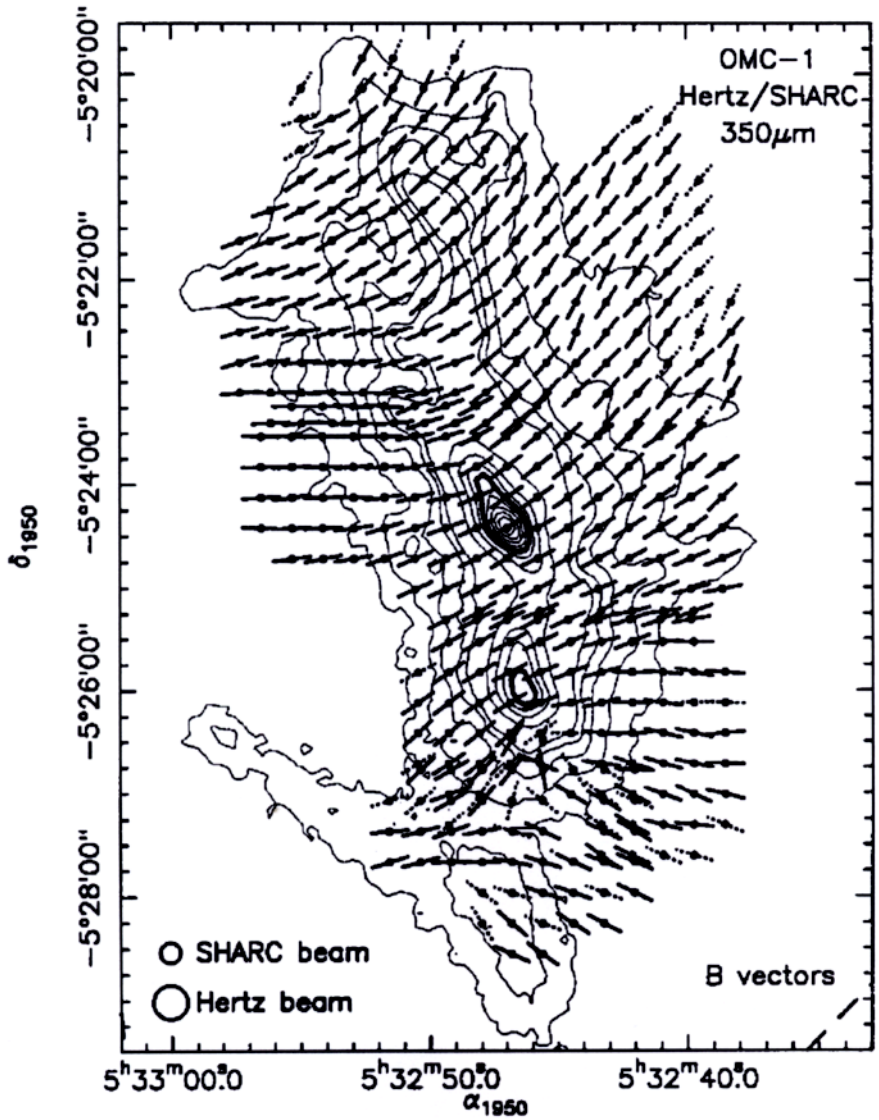
OMC−1
Hertz/SHARC
350μm
SHARC beam
Hertz beam
B vectors
−5°20'00"
−5°22'00"
−5°24'00"
−5°26'00"
−5°28'00"
δ1950
5h33m00s.0
5h32m50s.0
5h32m40s.0
α1950

Comparison of Heterodyne and Direct Detection Interferometers

- Same spectral resolution considerations as for single dish, but now spatial resolution much higher, so high spectral resolution even more important (for lines).

- Direct interferometer limited in number of telescopes (N) due to beamsplitting (N-1) which divides down the signal.

- Heterodyne detection interferometer – no limit to number of telescopes (except for $).